



Flow past a rectangular cylinder close to a free surface

Wenjie Zhong^a, Lu Deng^{a,b,*}, Zhiying Xiao^c

^a College of Civil Engineering, Hunan University, Changsha, 410082, Hunan, China

^b Key Laboratory for Damage Diagnosis of Engineering Structures of Hunan Province, Changsha, 410082, Hunan, China

^c Powerchina Kunming Engineering Corporation Limited, Kunming, 650051, Yunnan, China

ARTICLE INFO

Keywords:

Rectangular cylinder
Free surface
RANS simulation
Drag
Lift

ABSTRACT

Flow past rectangular cylinders represents an idealized flow around bluff bodies. Knowing the hydrodynamic properties of rectangular cylinders in a steady flow is of practical importance for many engineering applications. Although the unbounded flow past rectangular cylinders has been broadly studied, investigations on the flow around rectangular cylinders close to the free surface are limited. In the present study, two-dimensional multiphase simulations of flow past rectangular cylinders were conducted using RANS. The Mentor shear stress transport (SST) $k-\omega$ model and the volume of fluid (VoF) model were adopted. The Mentor SST $k-\omega$ model is capable of accurately predicting the flow past rectangular cylinders near the free surface when the width-to-length ratio is larger than 0.7. The effect of the depth-to-length ratio on the hydrodynamic properties of rectangular cylinders is affected by the width-to-length ratio and becomes significant when the depth-to-length ratio is lower than 1.0. The effect of the width-to-length ratio on the flow past rectangular cylinders near the free surface is different from that in an infinite domain. The findings from the present study can provide a deep understanding of the hydrodynamic properties of rectangular cylinders close to the free surface.

1. Introduction

Flow past rectangular cylinders in an infinite domain has been broadly investigated (Mannini et al., 2010, 2011; Schewe, 2013; Tian et al., 2013) due to its practical importance in engineering applications and scientific significance in fluid mechanics. Recently, research on the flow around rectangular cylinders has been extended to incorporate the effects of asymmetric boundary conditions, i.e., in the vicinity of the free surface. This type of flow is relevant for many civil and marine engineering applications, e.g., bridge decks (Malavasi and Guadagnini, 2003), offshore platform columns and hydrokinetic turbine blades (Liu et al., 2016). Understanding the hydrodynamic behaviors of rectangular cylinders under the effect of the free surface is an important consideration for offshore structure design.

Some studies on the flow past rectangular cylinders close to the free surface have been carried out. Liu et al. (2016) numerically investigated the flow past a plate with a width-to-length ratio of 0.1 in the vicinity of a free surface. They demonstrated that as the depth decreases, the wake structures behind the plate become irregular and a jet-like flow forms from the surface on top of the plate when the depth is $0.3l$ (where l is the length of the plate.). Similar flow structures have been observed by

Reichl et al. (2005) for a circular cylinder and by Mirauda et al. (2013) for a sphere. Mirauda et al. (2013) demonstrated that in the extreme case of $d = 0$, the vortex shedding around the sphere is suppressed by the free surface distortion, resulting in the enhancement of the vorticity intensity on the side regions of the obstacle. Liu et al. (2016) reported that the drag coefficient of the plate decreases as the depth decreases and a dramatic decrease of the drag coefficient occurs between a depth of $0.6l$ and $0.5l$. Similar variations of the drag coefficient with the depth were observed in the flow past circular cylinders near the free surface (Miyata et al., 1990). Malavasi and Guadagnini (2007) experimentally investigated the interaction between the free surface and a submerged rectangular cylinder with the width-to-length ratio of 3.0. Two important factors, i.e., the depth and the elevation from the floor, were considered in their study. Malavasi and Guadagnini (2007) reported that when the water depth is fixed at $7.0l$, the drag coefficient of the rectangular cylinder increases as the depth decreases from $4.5l$ to 0 while the lift coefficient approximately levels from $d = 4.5l$ to $d = 1.5l$ and decreases from $d = 1.5l$ to $d = 0$. It is found that the variations of the drag and lift coefficients with the depth reported by Malavasi and Guadagnini (2007) are different from those reported by Liu et al. (2016). An obvious distinction between the two studies (Liu et al., 2016; Miyata et al., 1990)

* Corresponding author. College of Civil Engineering, Hunan University, Changsha 410082, Hunan, China.
E-mail address: denglu@hnu.edu.cn (L. Deng).

<https://doi.org/10.1016/j.oceaneng.2019.106118>

Received 9 September 2018; Received in revised form 4 March 2019; Accepted 16 June 2019

Available online 1 July 2019

0029-8018/© 2019 Elsevier Ltd. All rights reserved.

is the difference of the width-to-length ratio, which may account for the disagreement.

The width-to-length ratio (w/l , where w and l are the width and length of the rectangular cylinder, respectively.) is an important factor affecting the flow structures and force coefficients of rectangular cylinders in a steady flow. Nakaguchi et al. (1968) reported a peak in the drag coefficient at around $w/l = 0.7$ and a discontinuity in the Strouhal number at around $w/l = 2.8$ for the Reynolds number ranging from 2.0×10^4 to 6.0×10^4 . This was also observed by Norberg (1993) who carried out wind tunnel experiments ($4.0 \times 10^2 < Re < 3.0 \times 10^4$) and Sohankar (2008) who conducted 3D LES simulations ($Re = 1.0 \times 10^5$). Shimada and Ishihara (2002) reported two discontinuities in the Strouhal number at $w/l = 2.8$ and $w/l = 6.0$ via using a modified RANS $k - \varepsilon$ model ($Re = 2.2 \times 10^4$). They found that the discontinuities in the Strouhal number are closely linked with the flow reattachment. Shimada and Ishihara (2002) indicated that as the width-to-length ratio increases from 0.6 to 8.0, the flow around rectangular cylinders successively shows “separated” ($w/l < 2.8$), “intermittently reattached” ($2.8 < w/l < 6.0$) and “fully reattached” ($6.0 < w/l$) patterns. Although the effect of the width-to-length ratio on the flow past rectangular cylinders in an infinite domain has been studied, there have been very few investigations on the effect of the width-to-length ratio when the rectangular cylinder approaches the free surface. Moreover, the effect of the depth-to-length ratio on the flow past rectangular cylinders with different width-to-length ratios and the relationship between the effects of the depth-to-length ratio and the width-to-length ratio of rectangular cylinders close to a free surface have not been well understood.

In the present study, numerical simulations of flow past rectangular cylinders near the free surface are conducted using the computational fluid dynamics (CFD) method. The Reynolds-averaged Navier-Stokes (RANS) approach is adopted. The turbulence is modeled with the Mentor shear stress transport (SST) $k - \omega$ model (Menter, 1994) and the free surface evolution is tracked with the volume of fluid (VoF) multiphase model (Hirt and Nichols, 1981). The applicability of the Mentor SST $k - \omega$ model (Menter, 1994) in modeling flow around rectangular cylinders near the free surface is discussed. The effects of the depth-to-length ratio (d/l , where d is the distance between the undisturbed surface and the top of the rectangular cylinder.) and the width-to-length ratio on the flow structures and force coefficients of rectangular cylinders are analyzed. A broad range of depth-to-length ratios (0.3–4.5) and width-to-length ratios (0.1–5.0) is considered in the numerical simulations. The significant effect of the free surface at $d/l \leq 1.0$ is observed and the existence of the critical depth-to-length ratio, below which the flow is dominated by the free surface effects, is identified. The effect of the depth-to-length ratio is found to be closely related to the width-to-length ratio of the rectangular cylinder. The findings from the present study can provide guidance on the multiphase simulations of flow around rectangular cylinders and contribute to the understanding of the hydrodynamic behaviors of structural members with rectangular cross-sections located close to the free surface. With this understanding, the proper depth can be determined for hydrokinetic turbines where the maximum drag force is obtained in order to maximize the power extraction, or the force coefficients of offshore platform columns at low depths ($d/l \leq 1.0$) can be estimated considering the significant free surface effects.

2. RANS turbulence model

RANS simulations using the Mentor SST $k - \omega$ model (Menter, 1994) are conducted in the present study. The RANS is a feasible solution for turbulence modeling in terms of computational requirements and can provide reasonable predictions for turbulent flows from engineering application perspective. The RANS has been successfully applied to high Reynolds number flows around plates (Liu et al., 2016) and cylinders (Mannini et al., 2010; Ong et al., 2009; Stringer et al., 2014; Tian et al., 2013). The Reynolds-averaged equations for the conservation of mass and momentum are given by

$$\frac{\partial u_i}{\partial x_j} = 0 \quad (1)$$

$$\frac{\partial u_i}{\partial t} + u_j \frac{\partial u_i}{\partial x_j} = -\frac{1}{\rho} \frac{\partial p}{\partial x_i} + \nu \frac{\partial^2 u_i}{\partial x_j^2} - \frac{\partial \overline{u_i' u_j'}}{\partial x_j} \quad (2)$$

where u_i and u_i' ($i = 1, 2, 3$) denote the mean velocity and fluctuating component of the velocity in the x_i direction, respectively. The averaged products of the fluctuating components $u_i' u_j'$ are the Reynolds stresses which result from the time-averaging of the nonlinear convection terms in the original Navier-Stokes (N-S) equations. In order to close the above equations, turbulence model is introduced. As the first step, the unknown Reynolds stress components are linearly related to the mean velocity using the Boussinesq approximation.

$$-\overline{u_i' u_j'} = \nu_t \left(\frac{\partial u_i}{\partial x_j} + \frac{\partial u_j}{\partial x_i} \right) - \frac{2}{3} k \delta_{ij} \quad (3)$$

where ν_t is the turbulent eddy viscosity and $k (= 0.5 u_i \overline{u_i'})$ is the turbulent kinetic energy. With the approximation, the calculation of the Reynolds stress is transferred to the computation of the turbulent eddy viscosity. In the present study, the two-equation Mentor SST $k - \omega$ model (Menter, 1994) is used to compute the turbulent eddy viscosity.

The Mentor SST $k - \omega$ model (Menter, 1994) is a mixture of the Wilcox $k - \omega$ model (Wilcox, 2006) and the standard $k - \varepsilon$ model (Jones and Launder, 1972), and has an improved adverse pressure gradient performance compared to other eddy-viscosity models (Moukalled et al., 2015). In the Mentor SST $k - \omega$ model (Menter, 1994), conservation equations of the turbulent kinetic energy k and the turbulent frequency ω are introduced.

$$\frac{\partial k}{\partial t} + u_j \frac{\partial k}{\partial x_j} = \frac{\partial}{\partial x_j} \left(\left(\nu + \frac{\nu_t}{\sigma_k} \right) \frac{\partial k}{\partial x_j} \right) + \frac{1}{\rho} \tilde{P}_k - \beta^* k \omega \quad (4)$$

$$\begin{aligned} \frac{\partial \omega}{\partial t} + u_j \frac{\partial \omega}{\partial x_j} = & \frac{\partial}{\partial x_j} \left(\left(\nu + \frac{\nu_t}{\sigma_\omega} \right) \frac{\partial \omega}{\partial x_j} \right) + \tilde{C}_\omega \frac{\omega}{k} \nu_t \left(\frac{\partial u_i}{\partial x_j} + \frac{\partial u_j}{\partial x_i} \right) \frac{\partial u_i}{\partial x_j} - \tilde{C}_\rho \omega^2 \\ & + 2(1 - F_1) \sigma_{\omega 2} \frac{1}{\omega} \frac{\partial k}{\partial x_j} \frac{\partial \omega}{\partial x_j} \end{aligned} \quad (5)$$

where \tilde{P}_k is the production of the turbulent kinetic energy and is calculated as

$$\tilde{P}_k = \text{Min} \left[\rho \nu_t \left(\frac{\partial u_i}{\partial x_j} + \frac{\partial u_j}{\partial x_i} \right) \frac{\partial u_i}{\partial x_j}, 10 \beta^* \rho k \omega \right] \quad (6)$$

The constants in the above equations are calculated by $\tilde{\phi} = F_1 \phi_1 + (1 - F_1) \phi_2$, where ϕ_1 and ϕ_2 are the corresponding constants in the original $k - \omega$ model and $k - \varepsilon$ model respectively. The blending function F_1 depends on the solution variables and the normal distance of the first internal grid point to the wall, and is calculated as

$$F_1 = \tanh(\gamma_1^4) \quad (7)$$

$$\gamma_1 = \text{Min} \left[\text{Max} \left(\frac{\sqrt{k}}{\beta^* \omega y}, \frac{500 \nu}{y^2 \omega} \right), \frac{4 \rho \sigma_{\omega 2} k}{CD_{k\omega} y^2} \right] \quad (8)$$

$$CD_{k\omega} = \text{Max} \left(2 \rho \sigma_{\omega 2} \frac{1}{\omega} \frac{\partial k}{\partial x_j} \frac{\partial \omega}{\partial x_j}, 10^{-10} \right) \quad (9)$$

with the constants of the original models assigned the following values: $C_{\alpha 1} = 0.5532$, $C_{\beta 1} = 0.075$, $\beta^* = 0.09$, $\sigma_{k1} = 2.00$, $\sigma_{\omega 1} = 2.00$, $C_{\alpha 2} = 0.4403$, $C_{\beta 2} = 0.0828$, $\sigma_{k2} = 1.00$ and $\sigma_{\omega 2} = 1.186$.

The turbulent eddy viscosity is computed by

$$\nu_t = \frac{0.31k}{\text{Max}(0.31\omega, \sqrt{2S}F_2)} \quad (10)$$

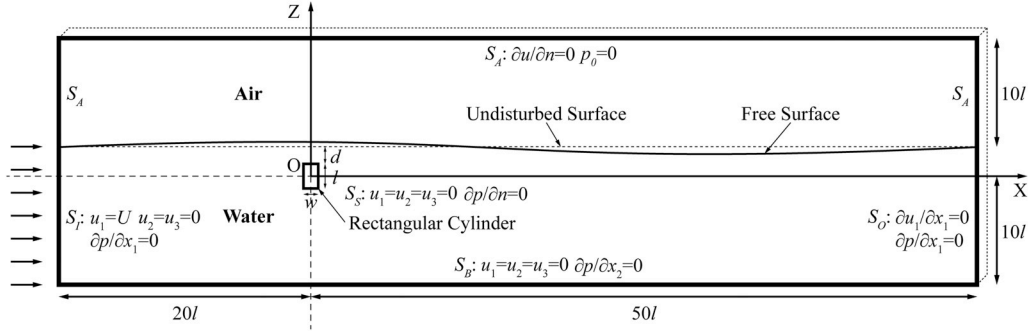


Fig. 1. The computational domain and the Cartesian coordinate system.

Table 1

Details of the parameters used in the simulations.

| Parameters | Symbol | Value |
|--|--------|--|
| Length of the rectangular cylinder | l | 0.10 m |
| Width of the rectangular cylinder | w | 0.01 m–0.50 m |
| Width-to-length ratio | w/l | 0.1–5.0 |
| Inlet velocity of the water | U | 0.25 m/s |
| Kinematic viscosity of the water | ν | $1.01 \times 10^{-6} \text{ m}^2/\text{s}$ |
| Reynolds number | Re | 2.5×10^4 |
| Density of the water | ρ | 1000 kg/m ³ |
| Distance between the undisturbed surface and the top of the rectangular cylinder | d | 0.03 m–0.45 m |
| Depth-to-length ratio | d/l | 0.3–4.5 |

where S_t is the magnitude of the strain rate and F_2 is given by $F_2 = \tanh(\gamma_2^2)$ with $\gamma_2 = \text{Max}(2k^{0.5}/\beta^* \omega y, 500\nu/y^2 \omega)$.

3. Computational overview

3.1. Computational domain and boundary conditions

Two-dimensional simulations of flow past rectangular cylinders near the free surface are conducted. The schematic of the computational domain and the Cartesian coordinate system of the model is drawn in Fig. 1. As shown in Fig. 1, the coordinate system is located in the center of the rectangular cylinder and the x axis is aligned with the inlet flow direction. The length of the computational domain is $70l$, which is larger than that by Liu et al. (2016). The inlet is $20l$ upstream the cylinder and the outlet is $50l$ downstream the cylinder. The distance between the cylinder and the outlet is believed to be sufficiently large that the outlet effects on the wake structures are negligible (Liu et al., 2016; Sohankar, 2008). The entire domain is composed of air on the top and water at the bottom. The top boundary is $10l$ away from undisturbed free surface and the bottom is $10l$ away from the center of the rectangular cylinder. The rectangular cylinder is placed below the free surface. The distance between the undisturbed surface and the top of the rectangular cylinder denoted by d has a significant impact on the flow structures and force coefficients of the cylinder. Details of the size of the rectangular cylinder along with other parameters used in the simulations are presented in Table 1.

The free surface evolution is tracked with the VoF method (Hirt and Nichols, 1981), in which a fluid volume fraction α is introduced. The α is bounded between 0 and 1, with $\alpha = 1$ representing water, $\alpha = 0$ representing air and $0 < \alpha < 1$ representing the air-water interface. The transport equation of the volume fraction is given by

$$\frac{\partial \alpha}{\partial t} + \frac{\partial u_j \alpha}{\partial x_j} = 0 \quad (11)$$

The fluid domain boundaries include the inlet S_I , the outlet S_O , the

atmosphere S_A , the bottom S_B and the structural surface S_S . The boundary conditions for the present simulations are shown in Fig. 1. At the inlet, a constant velocity $u_1 = U$ is imposed, and k and ω are calculated by

$$k = 1.5(UI)^2 \quad (12)$$

$$\omega = k^{0.5} / (C_\mu^{0.25} L) \quad (13)$$

where I ($= 5\%$) is the turbulence intensity and L ($= 0.07l$) is the turbulence length. The empirical constant C_μ is 0.09.

In the near-wall region, i.e., near the surface of the rectangular cylinder and at the bottom, if the flow is to be resolved, a considerable number of grid points will be required due to the large gradients of velocity. Wall functions are used in the near-wall region in the present simulations. With the use of wall functions, the turbulence model avoids the need to integrate all the way to the wall. The first internal grid point is placed in the logarithmic layer ($11.06 < y^+ < 200.00$). The empirical relations (Moukalled et al., 2015) in this layer are given by

$$u^+ = \frac{1}{\kappa} \text{Ln}(y^+) + B \quad (14)$$

$$k^+ = \frac{1}{\sqrt{C_\mu}} \quad (15)$$

$$\omega^+ = \frac{\nu}{\mu_\tau \kappa y \sqrt{C_\mu}} \quad (16)$$

where κ ($= 0.41$) is the von Karman constant and B is 5.25; y^+ ($= y\mu_\tau/\nu$), u^+ ($= u/u_\tau$), k^+ ($= k/u_\tau^2$) and ω^+ ($= \omega\nu/u_\tau^2$) represent the normalized distance to the wall, the normalized velocity parallel to the wall, the normalized turbulent kinetic energy and the normalized turbulent frequency, respectively; y is the normal distance from the first internal grid point to the wall and μ_τ is the friction velocity expressed in terms of the wall shear stress τ_w as $\mu_\tau = (\tau_w/\rho)^{0.5}$.

3.2. Numerical methods

The continuity and Reynolds-averaged N-S equations, the transport equation of volume fraction and the turbulence model equations are discretized using the finite volume method (FVM) performed in the open source package OpenFOAM. The FVM is implemented by integrating each term in the equations over a control volume and relating the volume integrals to the surface integrals using Gauss's theorem. The surface and volume integrals are both evaluated with the mid-point integration approximation which yields second order accuracy. Values at cell centers are linearly interpolated to values at face centers. The Laplacian and divergence terms are treated with the Gaussian linear corrected and Gaussian linear schemes, respectively. The second-order Crank-Nicolson (CN) scheme is used for the time integration.

The discretized equations are solved with the PIMPLE algorithm

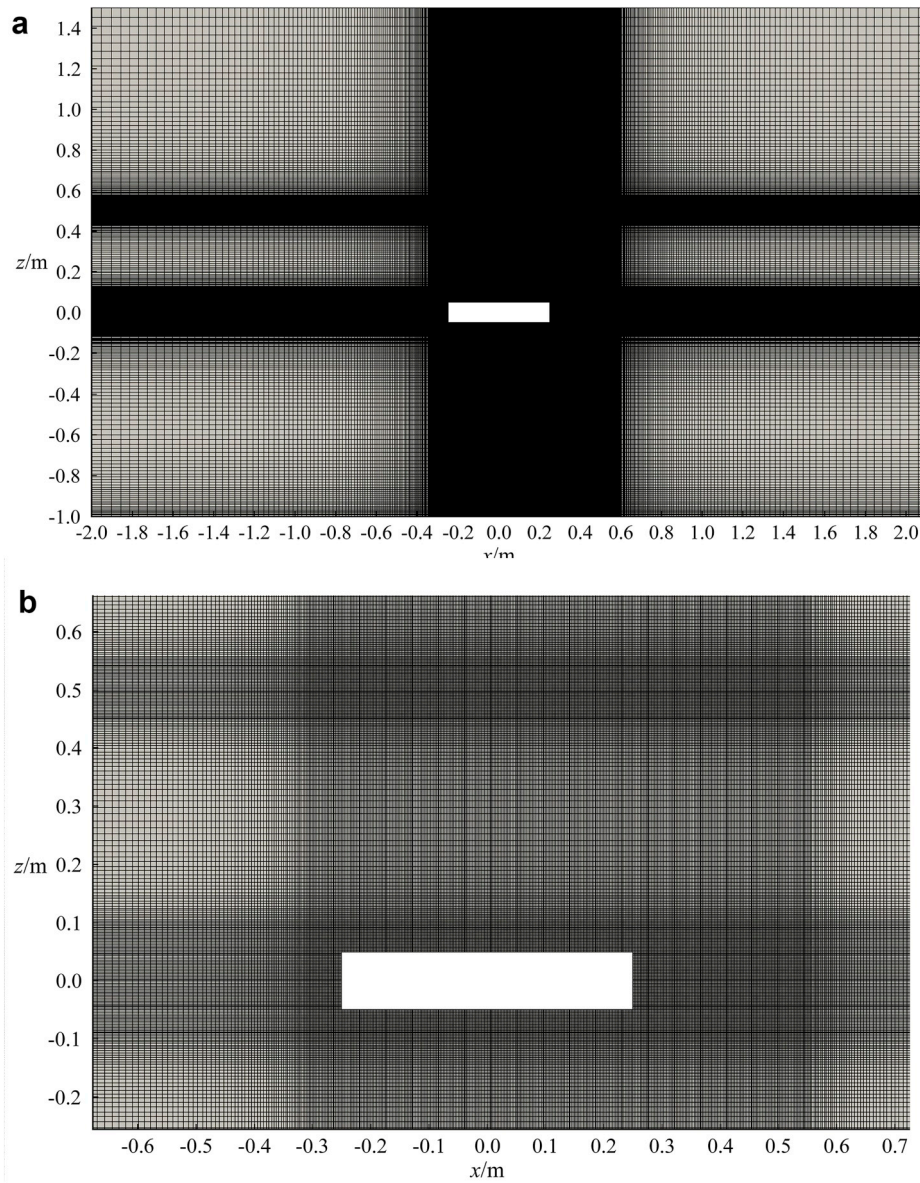


Fig. 2. The mesh generation: (a) Overall view; (b) Local view.

which is a hybrid of the PISO and SIMPLE algorithms. The principal of the algorithm is as follows (Holzmann, 2016): within each time step, both the inner pressure correction loop (PISO loop) and outer pressure-momentum correction loop (SIMPLE loop) are executed. In the inner loop, the pressure is recalculated with the new updated flux. In the

outer loop, the velocity matrix is first rebuilt with the new flux, the pressure is then corrected with the new velocity matrix and the flux is finally corrected with the new pressure. The calculations are repeated until convergence is achieved. In the present simulations, three inner loops and three outer loops are executed within each time step. The

Table 2
The mesh convergence study.

| Cases | No. | $\delta t U/l$ | Size | Grids | Elements | C_D | C_{Lrms} | St |
|----------------------------|----------------|----------------|------------------|------------------|----------|-------|------------|-------|
| $d/l = 0.3$ $w/l = 1.0$ | A ₁ | 0.0025 | $70l \times 20l$ | 390×220 | 169780 | 1.872 | 0.280 | 0.072 |
| | A ₂ | 0.0025 | $70l \times 20l$ | 425×235 | 198030 | 1.876 | 0.284 | 0.084 |
| | A ₃ | 0.0025 | $70l \times 20l$ | 459×255 | 232478 | 1.890 | 0.313 | 0.084 |
| $d/l = 0.3$ $w/l = 5.0$ | B ₁ | 0.0025 | $70l \times 20l$ | 539×220 | 223158 | 1.451 | 0.466 | 0.080 |
| | B ₂ | 0.0025 | $70l \times 20l$ | 585×235 | 261070 | 1.460 | 0.483 | 0.076 |
| | B ₃ | 0.0025 | $70l \times 20l$ | 619×255 | 301918 | 1.470 | 0.498 | 0.076 |
| $d/l = 4.5$ $w/l = 1.0$ | C ₁ | 0.0025 | $70l \times 25l$ | 379×308 | 231798 | 2.247 | 1.489 | 0.128 |
| | C ₂ | 0.0025 | $70l \times 25l$ | 425×323 | 273006 | 2.233 | 1.528 | 0.128 |
| | C ₃ | 0.0025 | $70l \times 25l$ | 459×342 | 312518 | 2.259 | 1.589 | 0.128 |
| $d/l = 4.5$ $w/l = 5.0$ | D ₁ | 0.0025 | $70l \times 25l$ | 539×308 | 318198 | 1.198 | 0.156 | 0.124 |
| | D ₂ | 0.0025 | $70l \times 25l$ | 585×323 | 364206 | 1.207 | 0.172 | 0.124 |
| | D ₃ | 0.0025 | $70l \times 25l$ | 619×342 | 409798 | 1.209 | 0.178 | 0.120 |

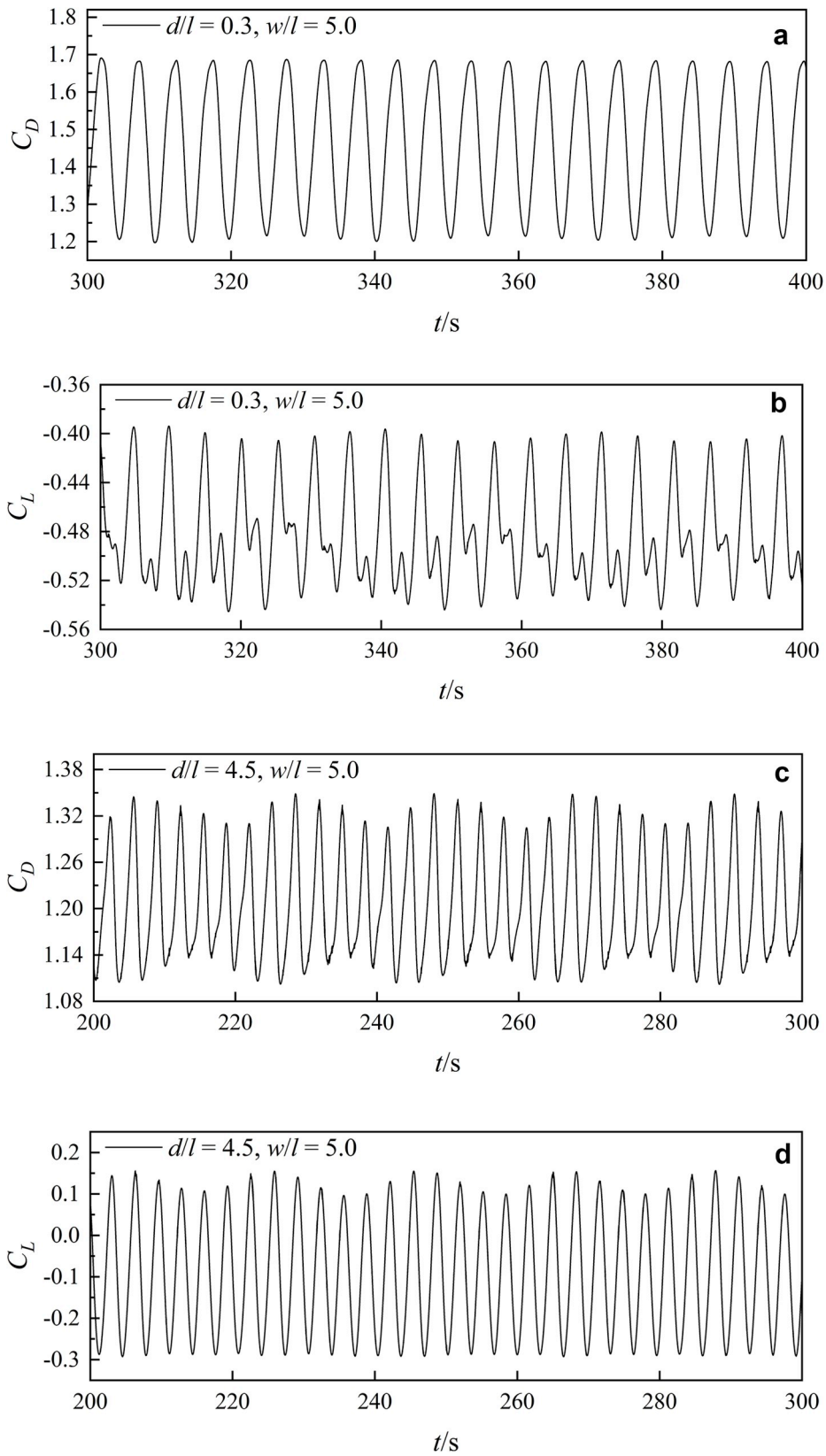


Fig. 3. The drag and lift coefficients as functions of time: (a) Drag coefficient ($d/l = 0.3$ and $w/l = 5.0$); (b) Lift coefficient ($d/l = 0.3$ and $w/l = 5.0$); (c) Drag coefficient ($d/l = 4.5$ and $w/l = 5.0$); (d) Lift coefficient ($d/l = 4.5$ and $w/l = 5.0$).

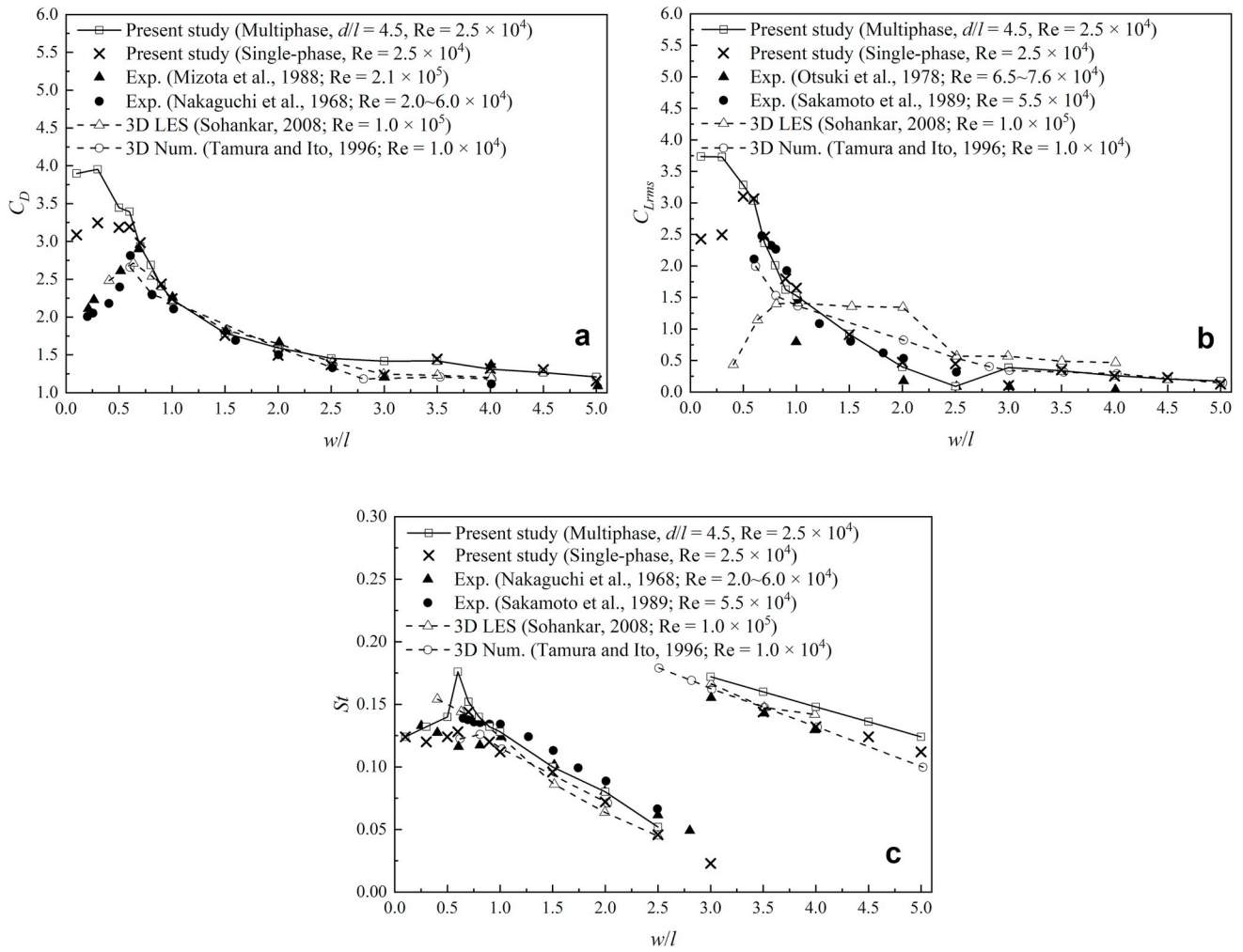


Fig. 4. Variations of the force coefficients of the rectangular cylinder with the width-to-length ratio: (a) Drag coefficient; (b) Lift coefficient (r.m.s.); (c) Strouhal number.

solutions are regarded as being converged when the final residuals of the velocity and pressure are lower than $1E-06$.

3.3. Grid convergence study

The meshes are generated by an algebraic method. With the prediction that significant vortex generations occur near the rectangular cylinder, grid points are intentionally clustered around the surface of the cylinder and stretch out gradually. The medium mesh for the case of $d/l = 4.5$ and $w/l = 5.0$ is presented in Fig. 2. As shown in Fig. 2, the grid is fully orthogonal and dense areas of the grid points appear in the region near the rectangular cylinder and the free surface.

The grid convergence study is conducted for four cases ($d/l = 0.3$ and $w/l = 1.0$; $d/l = 0.3$ and $w/l = 5.0$; $d/l = 4.5$ and $w/l = 1.0$; $d/l = 4.5$ and $w/l = 5.0$). Details of the meshes are presented in Table 2. The cases with subscripts 1, 2 and 3 represent coarse, medium and fine meshes, respectively. The drag and lift coefficients of rectangular cylinders are defined as

$$C_D = \frac{F_D}{0.5\rho U^2 l} \quad (17)$$

$$C_L = \frac{F_L}{0.5\rho U^2 w} \quad (18)$$

where F_D and F_L are the streamwise and cross-stream forces acting on the rectangular cylinder per unit length in the x_2 direction, respectively. The

root-mean-square (r.m.s.) value of the lift coefficient is calculated as

$$C_{Lrms} = \sqrt{\frac{C_{L1}^2 + C_{L2}^2 + C_{L3}^2 + \dots + C_{Ln}^2}{n}} \quad (19)$$

The drag and lift coefficients as functions of time for the cases with $w/l = 5.0$ are shown in Fig. 3. It is seen that the flow becomes stable after 300s when the depth is $0.3l$ while the stable flow emerges after 200s at the depth of $4.5l$. The same situations happen for the cases with $w/l = 1.0$. It seems that at low depth-to-length ratios, the flow takes a longer time to reach a stable condition. In the present study, the time-averaged drag and lift coefficients are calculated over the time period 300s–400s and 200s–300s when d/l is lower and higher than 1.0, respectively. Results of the convergence study are shown in Table 2. As shown in Table 2, the differences of the drag coefficient and Strouhal number obtained with medium and fine meshes are generally below 1%. For the r.m.s. value of the lift coefficient, a relatively large difference exists between the results obtained with three mesh densities (mostly around 3%). In the present study, simulations with medium mesh densities are chosen for all the cases in consideration of the tradeoff between accuracy and computing time.

It is noted that the distance of the first internal grid point to the wall denoted by y is selected to be $0.025l$ at the surface of the rectangular cylinder and $0.050l$ at the bottom. The averaged y^+ around the surface of the rectangular cylinder for meshes A_2 , B_2 , C_2 and D_2 are 17.8, 15.9, 18.2 and 11.8 respectively, indicating that the first internal grid points are

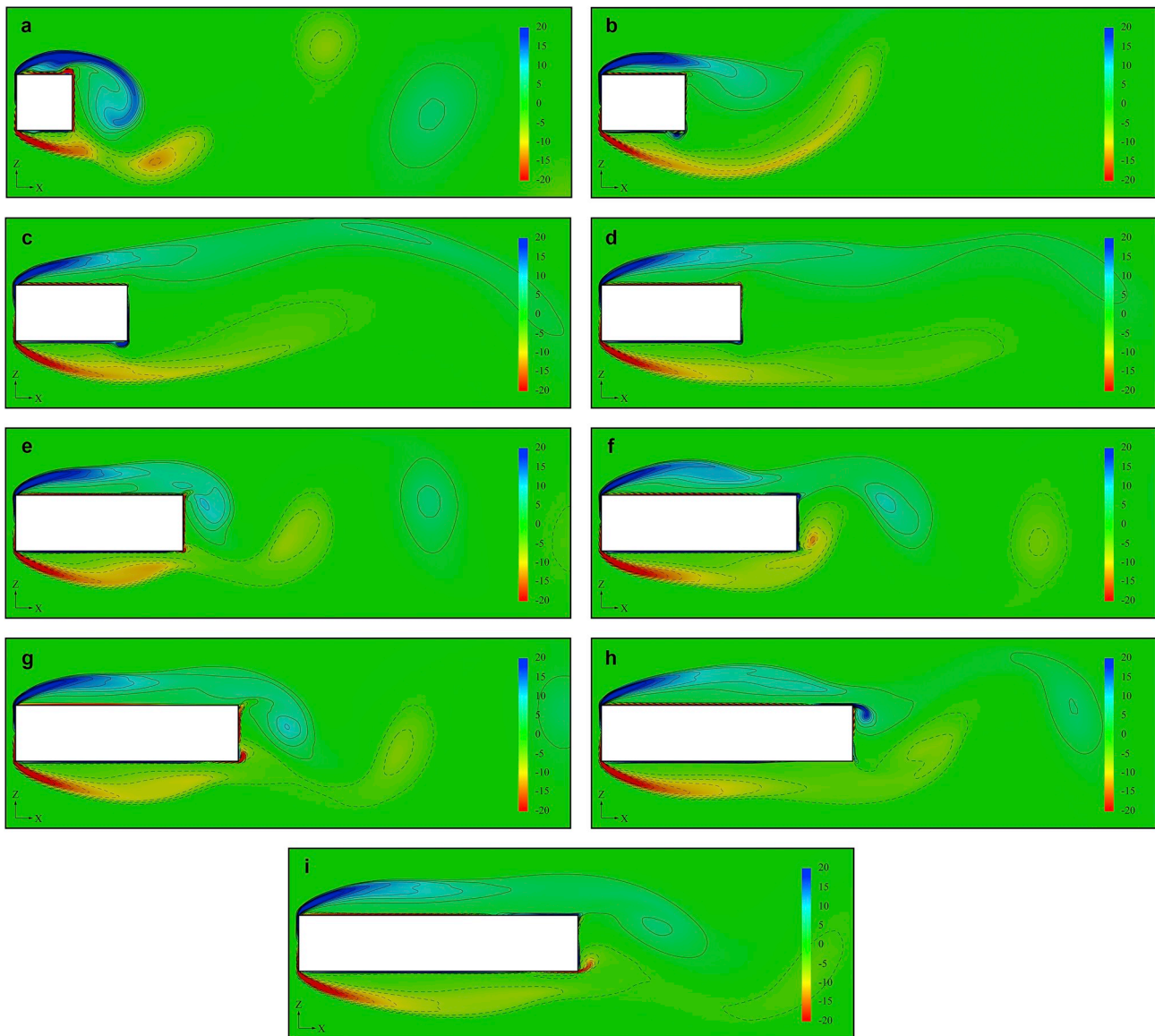


Fig. 5. Vorticity contours around the rectangular cylinder at various width-to-length ratios ($d/l = 4.5$): (a) $w/l = 1.0$; (b) $w/l = 1.5$; (c) $w/l = 2.0$; (d) $w/l = 2.5$; (e) $w/l = 3.0$; (f) $w/l = 3.5$; (g) $w/l = 4.0$; (h) $w/l = 4.5$; (i) $w/l = 5.0$.

generally located in the logarithmic layer.

4. Results and discussion

4.1. Applicability of the RANS turbulence model

In order to study the applicability of the Mentor SST $k - \omega$ model (Menter, 1994) in modeling flow past rectangular cylinders, the predicted hydrodynamic results of this study are compared with the published results (Mizota et al., 1988; Nakaguchi et al., 1968; Ohtsuki, 1978; Sakamoto et al., 1989; Sohankar, 2008; Tamura and Itoh, 1996). The drag and lift coefficients are calculated by Eq. (17) and Eq. (18). The Strouhal number is defined as $St = fl/U$ (where f denotes the vortex shedding frequency). Both the results obtained from the single-phase and multiphase simulations are presented in Fig. 4(a) - (c). In the multiphase simulations, the rectangular cylinder is placed at a depth of $4.5l$ below the water surface. With d/l equal to 4.5, the influence of the free surface on the force coefficients of rectangular cylinders is considered to be negligible (Malavasi and Guadagnini, 2007).

The drag coefficient of the rectangular cylinder with different width-

to-length ratios is depicted in Fig. 4(a). As shown in Fig. 4(a), the peak in the drag coefficient at around $w/l = 0.7$ is acquired through both the experiments (Mizota et al., 1988; Nakaguchi et al., 1968) and simulations (Sohankar, 2008; Tamura and Itoh, 1996). Fig. 4(a) shows that the drag coefficient predicted by using the single-phase model agrees well with the published results when w/l is between 0.7 and 5.0. This is consistent with that reported by Tian et al. (2013). Fig. 4(a) also shows that the drag coefficient obtained from the multiphase simulations is in good agreement with the published results when w/l is between 0.7 and 5.0. However, when w/l is lower than 0.7, the predicted drag coefficient is larger than both the experimental and numerical results. The over-estimation probably stems from the adoption of 2D modeling, with which the significant three-dimensional effects at low width-to-length ratios are neglected (Mannini et al., 2010; Shur et al., 2005).

Fig. 4(b) shows that the r.m.s. value of the lift coefficient decreases and the rate of decline decreases as w/l increases from 0.7 to 5.0. However, when w/l is lower than 0.7, the r.m.s. value increases with w/l . This variation trend is roughly captured via adopting the Mentor SST $k - \omega$ model (Menter, 1994) in both the single-phase and multiphase simulations. However, when w/l is lower than 0.7, the r.m.s. value of the lift

Table 3
The force coefficients of the square.

| Reference | Method | Re | C_D | C_{Lrms} | St |
|-----------------------------|------------------------------|-------------------|-------|------------|-------|
| Present study | SST $k - \omega$ (2D) | 2.5×10^4 | 2.233 | 1.528 | 0.128 |
| Lyn et al. (1995) | Exp. | 2.1×10^4 | 2.100 | / | 0.132 |
| Farhadi and Rahnama (2005) | LES (3D) | 2.1×10^4 | 2.306 | 0.984 | 0.138 |
| Murakami and Mochida (1995) | LES (3D) | 2.2×10^4 | 2.090 | 1.600 | 0.132 |
| Tian et al. (2013) | SST $k - \omega$ (2D) | 2.1×10^4 | 2.060 | 1.492 | 0.138 |
| Bosch and Rodi (1998) | $k - \epsilon$ (2D) | 2.2×10^4 | 2.108 | 1.012 | 0.146 |
| Shimada and Ishihara (2002) | Modified $k - \epsilon$ (2D) | 2.2×10^4 | 2.050 | 1.430 | 0.141 |

coefficient is overpredicted by using the $k - \omega$ model. It indicates that the multiphase simulations with the Mentor SST $k - \omega$ model (Menter, 1994) are incapable of accurately predicting the force coefficients of rectangular cylinders when $w/l < 0.7$.

Fig. 4(c) shows that the Strouhal number obtained from both the single-phase and multiphase simulations is in good agreement with the published results (Nakaguchi et al., 1968; Sakamoto et al., 1989; Sohankar, 2008; Tamura and Itoh, 1996). The discontinuity in the Strouhal number appearing at around $w/l = 2.8$ is acquired by the present RANS simulations. It indicates that the flow past rectangular cylinders is reasonably reproduced via using the Mentor SST $k - \omega$ model (Menter, 1994). In order to study the flow structures, the flow around rectangular cylinders is visualized by vorticity contours as depicted in

Fig. 5. The vorticity contours are obtained from the multiphase simulations and are plotted at 16 levels of $\omega_2 (= \pm 2.5 \text{ s}^{-1}, \pm 5.0 \text{ s}^{-1}, \pm 7.5 \text{ s}^{-1}, \pm 10.0 \text{ s}^{-1}, \pm 12.5 \text{ s}^{-1}, \pm 15.0 \text{ s}^{-1}, \pm 17.5 \text{ s}^{-1}, \pm 20.0 \text{ s}^{-1})$. The solid and dashed contour lines represent the positive and negative vorticity contours, respectively. The vorticity component in the x_2 direction is defined as

$$\omega_2 = \frac{\partial u_1}{\partial x_3} - \frac{\partial u_3}{\partial x_1} \quad (20)$$

Flow visualizations depicted in Fig. 5 are in agreement with those reported by Shimada and Ishihara (2002). Fig. 5(a)–(d) show that when w/l is lower than 2.5, the rectangular cylinder is immersed in the separated flow region. No flow reattachment is displayed due to the small widths of the cross-sections. Fig. 5(a)–(d) also show that as w/l increases from 1.0 to 2.5, the location of the vortex behind the rectangular cylinder moves further downstream and the vortex becomes weaker. This is an illustration of the decrease of the Strouhal number when w/l increases from 1.0 to 2.5 as shown in Fig. 4(c). It is seen from Fig. 5(e)–(i) that when w/l falls between 3.0 and 5.0, the flow separating from the upper and lower corners of the leading edge reattaches the side surfaces of the rectangular cylinder. A substantial change of the flow occurs as w/l increases from 2.5 to 3.0. With the change of the flow, the vortex shedding frequency rises suddenly, resulting in the discontinuity in the Strouhal number (see Fig. 4(c)).

The force coefficients of the square obtained from the present multiphase simulations are compared with the published results (Lyn et al., 1995; Bosch and Rodi, 1998; Farhadi and Rahnama, 2005;

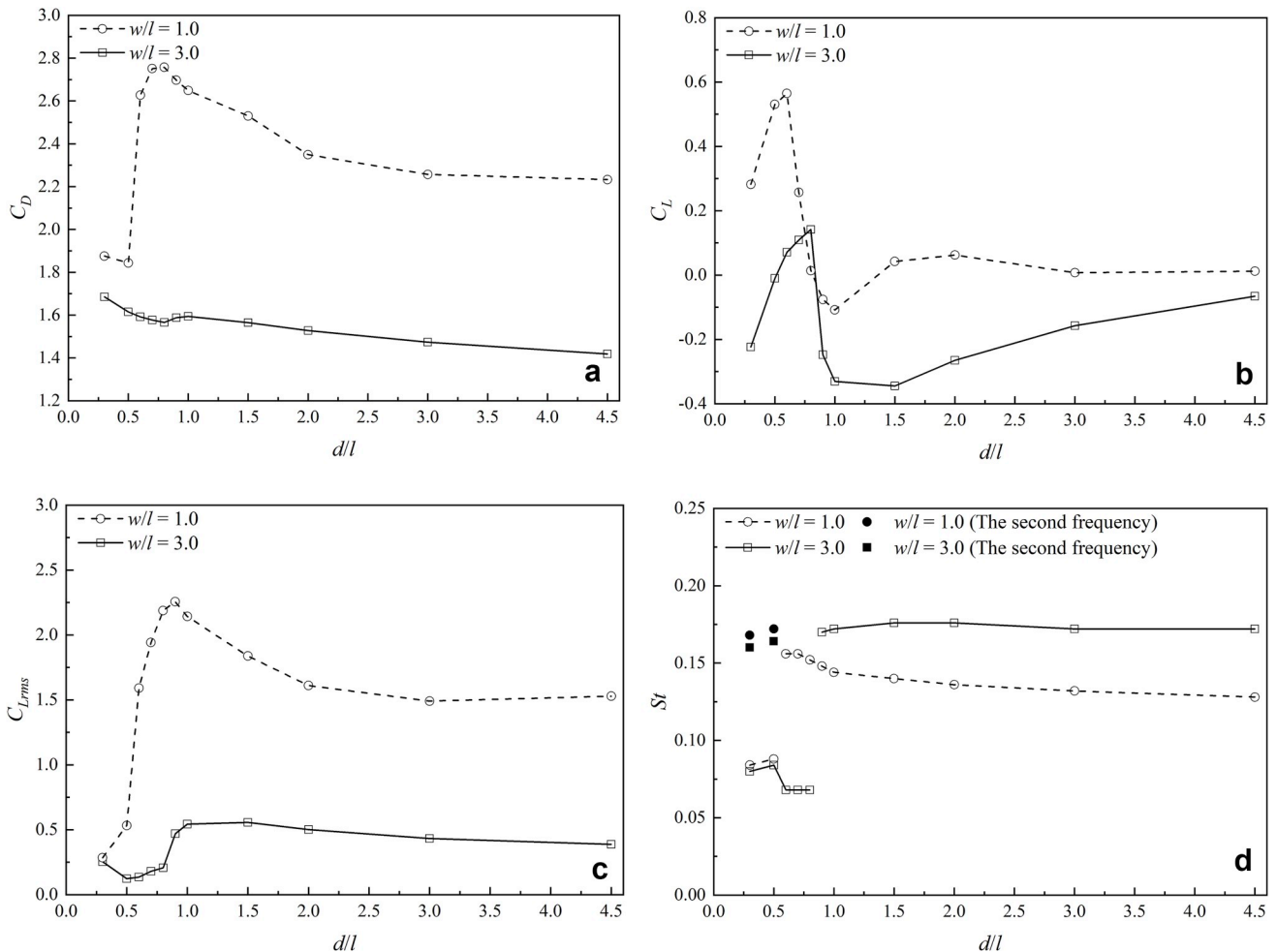


Fig. 6. Variations of the force coefficients of the rectangular cylinder with the depth-to-length ratio: (a) Drag coefficient; (b) Lift coefficient; (c) Lift coefficient (r.m.s.); (d) Strouhal number.

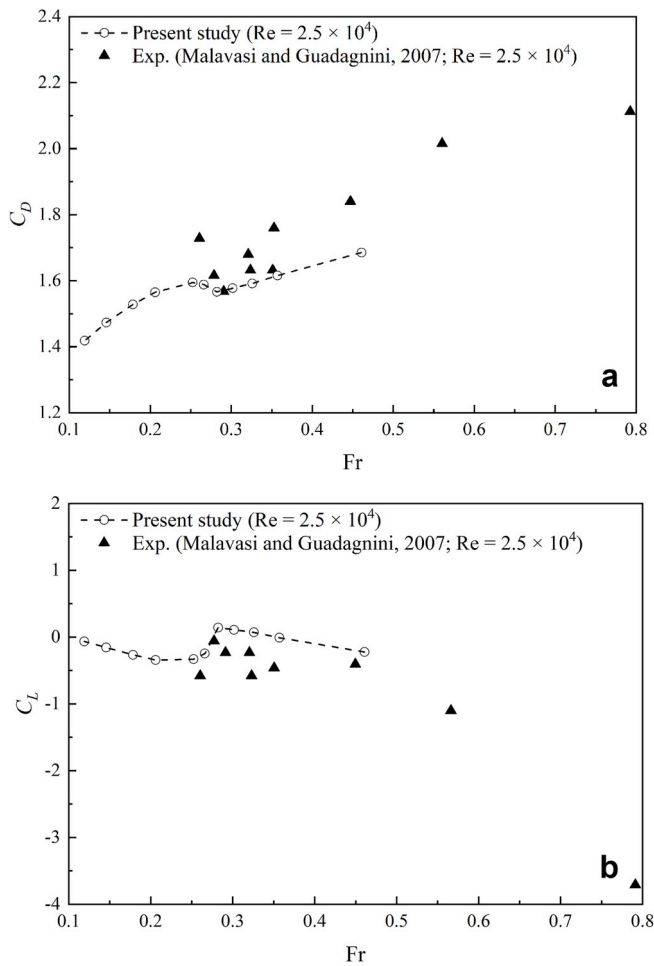


Fig. 7. Variations of the force coefficients of the rectangular cylinder with the Froude number ($w/l = 3.0$): (a) Drag coefficient; (b) Lift coefficient.

Murakami and Mochida, 1995; Shimada and Ishihara, 2002; Tian et al., 2013). As shown in Table 3, the predicted drag coefficient and r.m.s. value of the lift coefficient agree well with the numerical results by Farhadi and Rahnama (2005) and Murakami and Mochida (1995), respectively. However, it is seen that there are discrepancies between the predicted drag and lift coefficients of this study and the results reported by Lyn et al. (1995), Tian et al. (2013), Bosch and Rodi (1998) and Shimada and Ishihara (2002). The differences between the results are probably due to the different settings in the experimental or numerical studies, e.g., the spanwise extension and blockage ratio. Table 3 also shows that the predicted Strouhal number of this study is in good agreement with the published results.

4.2. Effect of the depth-to-length ratio

The effect of the depth-to-length ratio on the hydrodynamic properties of rectangular cylinders with width-to-length ratios of 1.0 and 3.0 is discussed in this section. As mentioned above, the unbounded flow past rectangular cylinders with width-to-length ratios of 1.0 and 3.0 shows “separated” and “intermittently reattached” patterns, respectively (Shimada and Ishihara, 2002). As the rectangular cylinder approaches the water surface, the free surface effects on the cylinder with the two w/l values are different as will be presented in the following paragraphs.

The drag coefficient of the rectangular cylinder at various depth-to-length ratios is depicted in Fig. 6(a). As shown in Fig. 6(a), when w/l is 1.0, the drag coefficient increases as d/l decreases from 4.5 to 0.8 and

drops sharply when d/l decreases from 0.8 to 0.5. Then, the drag coefficient increases slightly with d/l decreasing from 0.5 to 0.3. The maximum drag coefficient ($C_d = 2.757$) appears at the depth of $0.8l$ and is distinctly larger than that ($C_d = 2.233$) at $d/l = 4.5$. However, when w/l is 3.0, the drag coefficient increases as d/l decreases from 4.5 to 1.0, followed by a gentle reduction when d/l decreases from 1.0 to 0.8. The drag coefficient increases again as d/l decreases from 0.8 to 0.3, during which the growth rate of the drag coefficient is larger than that when d/l decreases from 4.5 to 1.0. It is predicted that the maximum drag coefficient of the rectangular cylinder ($w/l = 3.0$) will be obtained in the extreme case of $d = 0$. Fig. 6(a) also reveals that the variation trends of the drag coefficient with d/l at the two w/l values are similar, but the amplitudes of variation and the corresponding ranges of d/l values are different. These differences are likely attributed to the different intensities of interaction between the free surface and the rectangular cylinder at $w/l = 1.0$ and $w/l = 3.0$. As discussed previously, the flow past rectangular cylinders with width-to-length ratios of 1.0 and 3.0 in an infinite domain shows “separated” and “intermittently reattached” patterns, respectively (Shimada and Ishihara, 2002). When the cylinder approaches a water surface, the interaction between the free surface and the vortex shedding past the rectangular cylinder varies with the w/l value, leading to the different variations of the drag coefficient with d/l . The predicted results for the drag coefficient (at $w/l = 3.0$) of this study are compared with the experimental results by Malavasi and Guadagnini (2007). It is found that the present predicted drag coefficient is generally lower than that by Malavasi and Guadagnini (2007) at the same depth-to-length ratios. This is due to the different sizes of the rectangular cylinder in the two studies. In order to make comparisons between the results, the Froude number ($Fr = U/(gd)^{0.5}$) which allows the sole effect of the free surface to be examined is used as the x -coordinate. As shown in Fig. 7(a), the drag coefficient obtained from the present RANS simulations agrees well with the experimental results (Malavasi and Guadagnini, 2007) at $Fr < 0.4$. However, when Fr is larger than 0.4, the predicted drag coefficient is evidently smaller than the results by Malavasi and Guadagnini (2007). This is due to the different blockage ratios adopted in the present simulations ($\leq 9.3\%$) and by Malavasi and Guadagnini (2007) (14.3%).

Fig. 6(b) shows the variations of the lift coefficient with the depth-to-length ratio. It is seen from Fig. 6(b) that when w/l is 1.0, the lift coefficient varies slightly as d/l decreases from 4.5 to 1.5 and descends suddenly when d/l decreases from 1.5 to 1.0. The lift coefficient undergoes a sharp rise and fall as d/l decreases from 1.0 to 0.3, with the peak emerging at $d/l = 0.6$. Similar variations of the lift coefficient with d/l can be seen when w/l is 3.0, excepting that the lift coefficient decreases as d/l decreases from 4.5 to 1.5. It is important to note that the lift coefficient at both values of w/l ($w/l = 1.0$ and $w/l = 3.0$) varies remarkably in the d/l range from 1.0 to 0.3. Specifically, the sharp rise of the lift coefficient begins at $d/l = 1.0$ and ends at $d/l = 0.6$ when w/l is 1.0, while when w/l is 3.0, the lift coefficient starts rising at $d/l = 1.0$ and peaks at $d/l = 0.8$. It implies that the free surface effects become significant when the depth of the rectangular cylinder is lower than $1.0l$. This is also reflected by the dramatic decrease of the r.m.s. value of the lift coefficient in the corresponding d/l ranges as shown in Fig. 6(c). The sudden fall of the lift coefficient occurs in the d/l ranges from 0.6 to 0.3 and from 0.8 to 0.3 for rectangular cylinders with width-to-length ratios of 1.0 and 3.0, respectively. At these d/l ranges, the vortex shedding around the rectangular cylinder is totally different from that in an infinite domain as will be discussed later. Moreover, the predicted lift coefficient (at $w/l = 3.0$) of the present study is compared with the experimental results by Malavasi and Guadagnini (2007), and the results match well with each other as shown in Fig. 7(b).

Fig. 6(d) shows that for most depth-to-length ratios, the Strouhal number varies slightly with d/l . The dramatic variation of the Strouhal number occurs around the depth of $0.6l$ and $0.9l$ for rectangular cylinders with width-to-length ratios of 1.0 and 3.0, respectively. It indicates a substantial change of the flow at the two depths, and explains

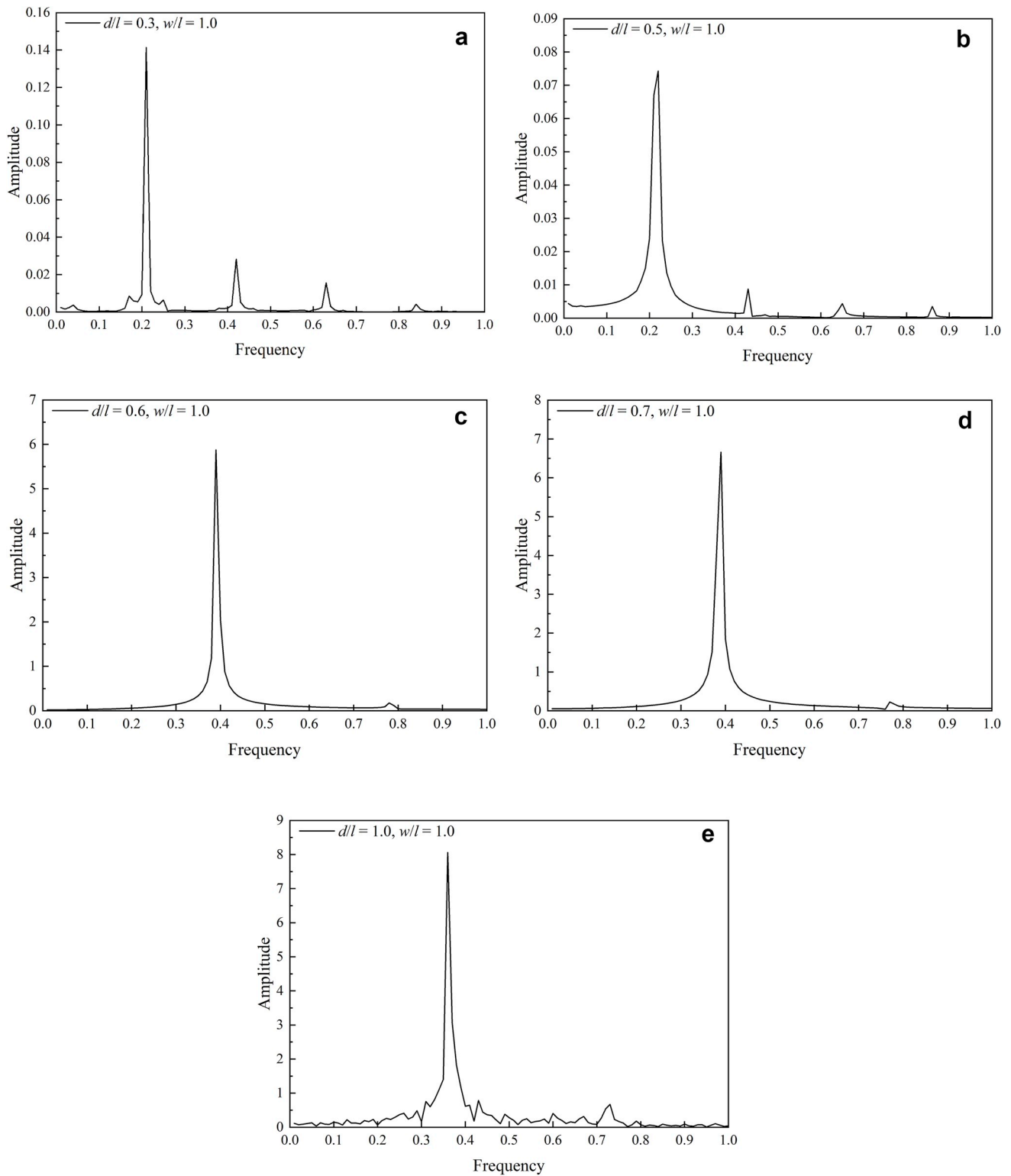


Fig. 8. Power spectra of the lift force ($w/l = 1.0$): (a) $d/l = 0.3$; (b) $d/l = 0.5$; (c) $d/l = 0.6$; (d) $d/l = 0.7$; (e) $d/l = 1.0$.

well the sharp rise of the lift coefficient with decreasing d/l at around the two depths. The relatively low values of Strouhal number in the d/l ranges from 0.5 to 0.3 and from 0.8 to 0.3 for rectangular cylinders at $w/l = 1.0$ and $w/l = 3.0$ imply that at these d/l ranges, the free surface effects play a dominant role on the vortex shedding around rectangular cylinders and the flow is totally different from that in an infinite domain. Fig. 8 and Fig. 9 show the frequency distribution of the lift force for the cases with $w/l = 1.0$ and $w/l = 3.0$ at various depth-to-length ratios,

respectively. It is seen that the peak frequency varies dramatically as d/l decreases from 0.6 to 0.5 when w/l is 1.0 and from 0.9 to 0.8 when w/l is 3.0. This is in accordance with the variation of the Strouhal number with d/l (see Fig. 6(d)). It is also observed that at low depth-to-length ratios, the second largest peak is noticeable. These frequency values are depicted with mark symbols in Fig. 6(d). As shown in Fig. 6(d), the resultant Strouhal number of the second frequency at low d/l values approximates that at high d/l values. It reflects the fact that the flow

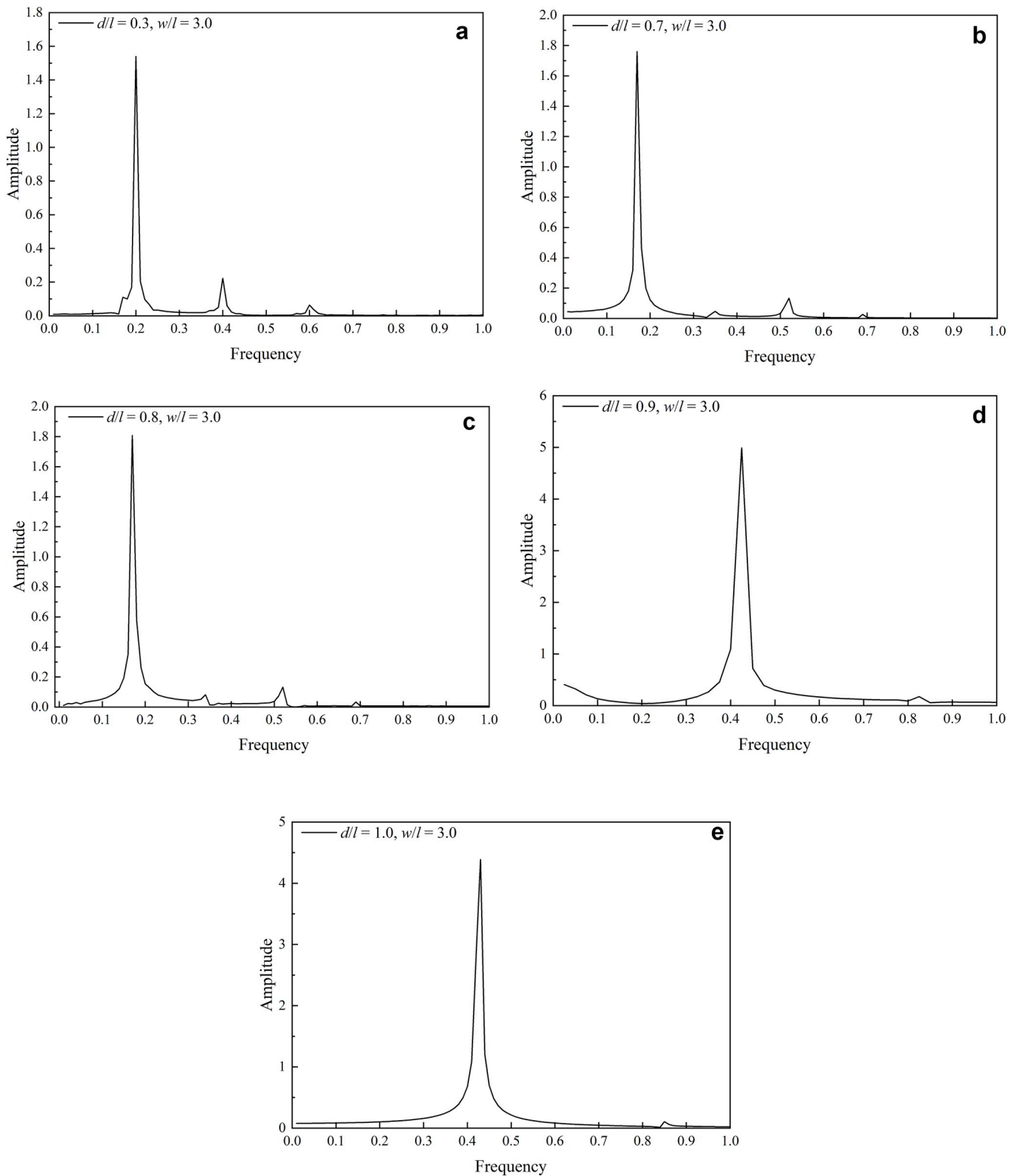


Fig. 9. Power spectra of the lift force ($w/l = 3.0$): (a) $d/l = 0.3$; (b) $d/l = 0.7$; (c) $d/l = 0.8$; (d) $d/l = 0.9$; (e) $d/l = 1.0$.

around rectangular cylinders near a free surface partly retains the features of the unbounded flow past rectangular cylinders, although the vortex shedding is markedly suppressed by the free surface distortion as indicated by the reduced amplitude of the second largest peak.

The vorticity contours around the rectangular cylinder at various depth-to-length ratios are depicted in Fig. 10 and Fig. 11. The black thick lines above the rectangular cylinder represent the free surface in the

figures. By comparing Fig. 10(e) to Fig. 5(a), it is observed that the flow around the rectangular cylinder ($w/l = 1.0$) at the depth of $1.0l$ is similar to that in an infinite domain. However, the vortices shed along the upper surface of the square are pressed due to the presence of the free surface. Reciprocally, the free surface on top of the square fluctuates slightly. This demonstrates the weak interaction between the free surface and the square. As d/l decreases from 1.0 to 0.6, the interaction between the free

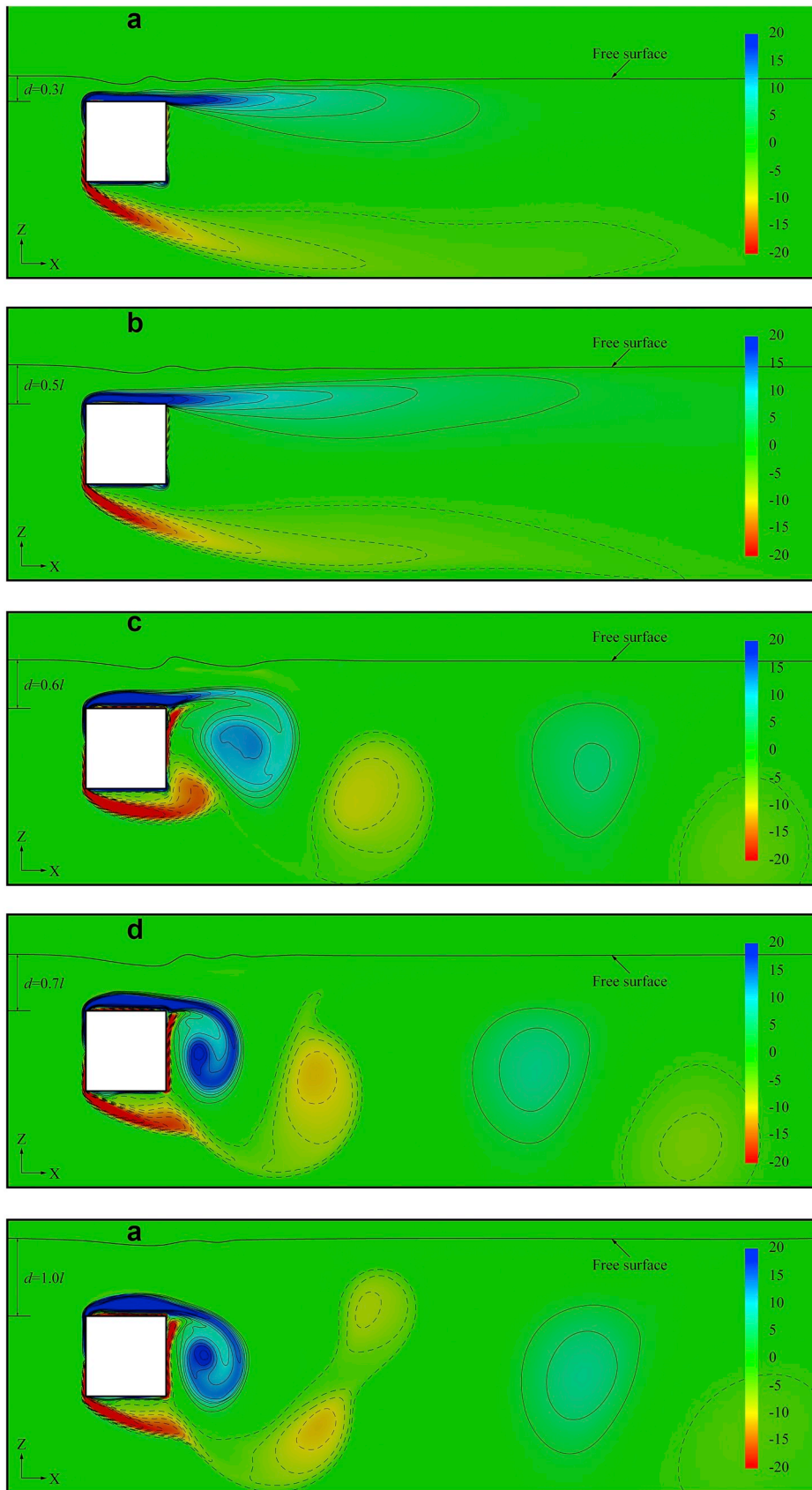


Fig. 10. Vorticity contours around the rectangular cylinder at various depth-to-length ratios ($w/l = 1.0$): (a) $d/l = 0.3$; (b) $d/l = 0.5$; (c) $d/l = 0.6$; (d) $d/l = 0.7$; (e) $d/l = 1.0$.

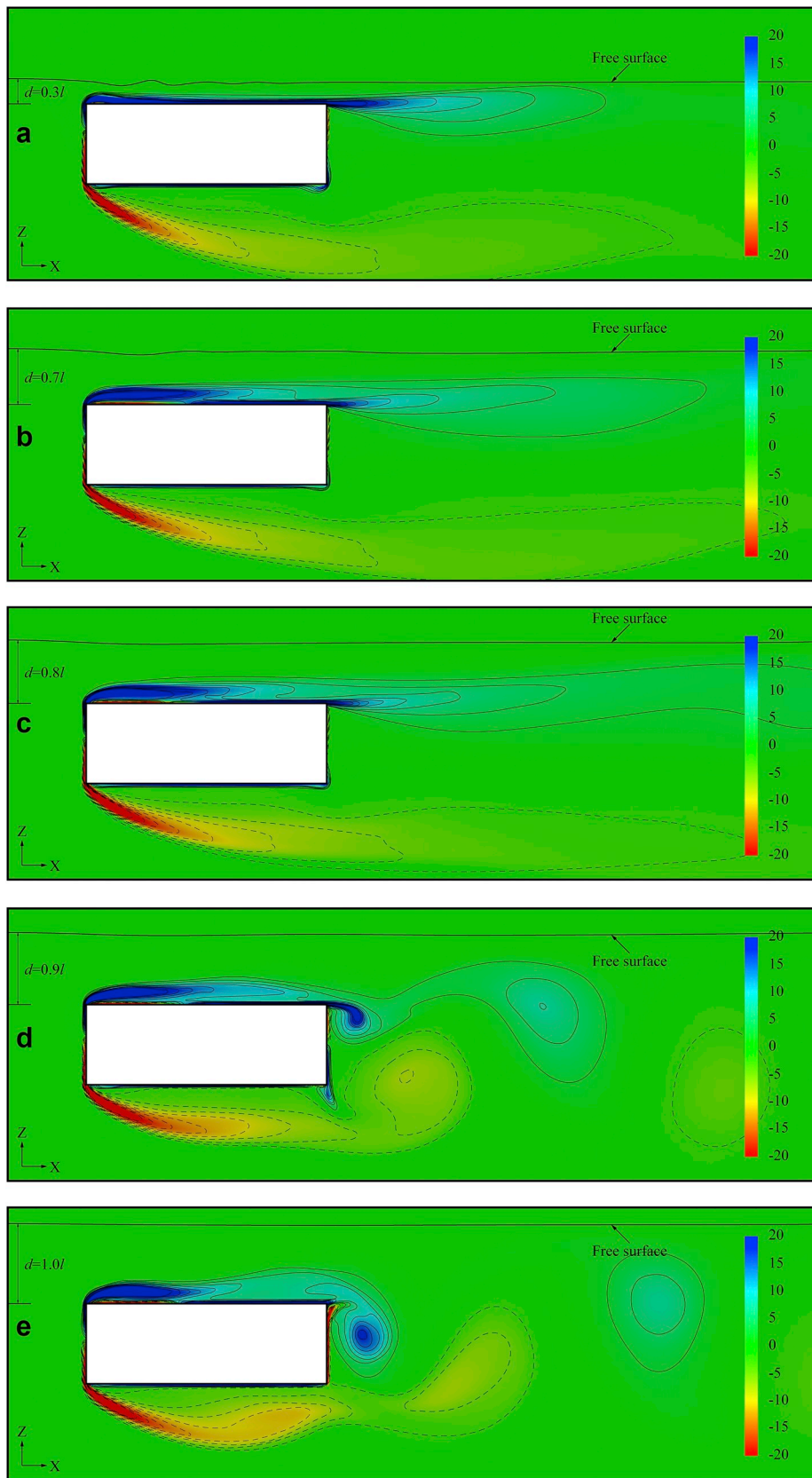


Fig. 11. Vorticity contours around the rectangular cylinder at various depth-to-length ratios ($w/l = 3.0$): (a) $d/l = 0.3$; (b) $d/l = 0.7$; (c) $d/l = 0.8$; (d) $d/l = 0.9$; (e) $d/l = 1.0$.

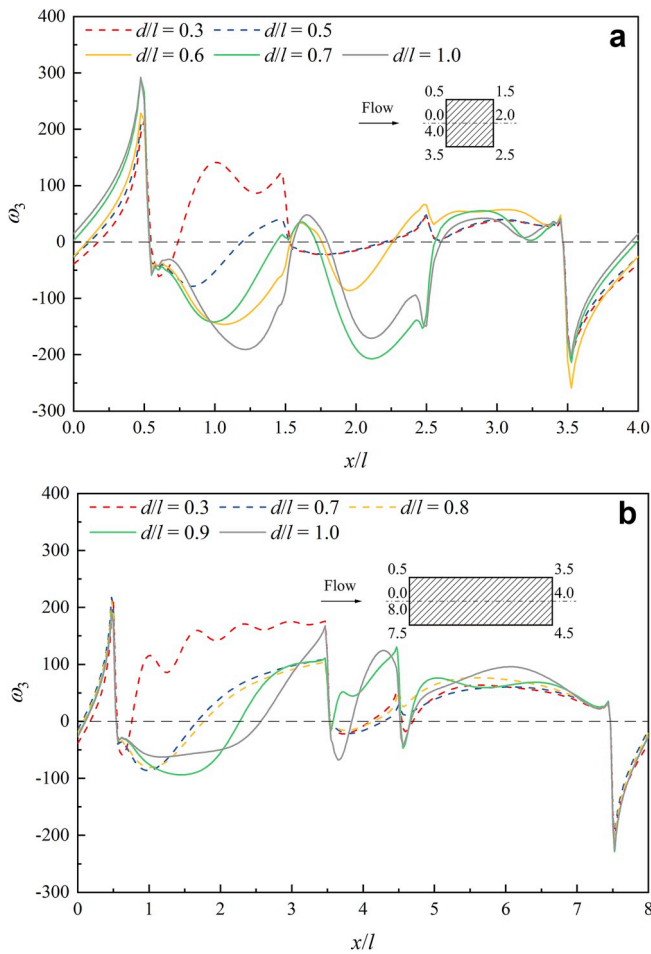


Fig. 12. Distributions of the time-averaged vorticity around the rectangular cylinder: (a) $w/l = 1.0$; (b) $w/l = 3.0$.

surface and the square becomes stronger. As shown in Fig. 10(c)–(e), with the approaching of the free surface, the vorticity contours above the square are flattened and fluctuations of the free surface increase. Meanwhile, the vortex shedding frequency rises as is reflected by the shortened distance between the successively shed positive or negative vortices. It results in the increase of the Strouhal number when d/l decreases from 1.0 to 0.6 as shown in Fig. 6(d). Fig. 10(a) and (b) show that when the square is submerged at the depth of $0.3l$ and $0.5l$, the flow around the square is completely different from that in an infinite domain. As shown in Fig. 10(a) and (b), the vortices shed from the upper corner of the leading edge are significantly pressed and the vortices generated at the lower corner of the leading edge are shed in a direction away from the lower surface of the square. With the vorticity contours elongated, the vortex shedding frequency drops, leading to the drastic reduction of the Strouhal number as d/l decreases from 0.6 to 0.5 (see Fig. 6(d)).

The vorticity contours around the rectangular cylinder ($w/l = 3.0$) at various depth-to-length ratios are shown in Fig. 11. It is seen from Fig. 11(e) that when d/l is 1.0, the flow around the rectangular cylinder reattaches the upper and lower surfaces. This is similar to that in an infinite domain (see Fig. 5(e)), except that the vortices above the rectangular cylinder are pressed under the effect of the free surface. Fig. 11(d) shows that when d/l is 0.9, positive vortices are generated at both the upper and lower corners of the trailing edge, causing the negative vortices under the rectangular cylinder to separate from the lower surface. As d/l decreases from 0.9 to 0.8, the free surface effects become more significant. Fig. 11(c) shows that the vorticity contours along the upper surface are flattened and lengthened, and the vorticity contours

along the lower surface are forced to stretch downward away from the rectangular cylinder. It is observed that the flow above the rectangular cylinder reattaches the upper surface while the flow below the rectangular cylinder separates from the lower corner of the leading edge without reattaching the lower surface. This causes the drop in vortex shedding frequency, leading to a dramatic decrease in Strouhal number (see Fig. 6(d)). Fig. 11(a)–(c) show that as d/l decreases from 0.8 to 0.3, the flow around the rectangular cylinder experiences small changes, with the vorticity contours shortened slightly.

Distributions of the time-averaged vorticity on the surfaces of the rectangular cylinder are depicted in Fig. 12. The distance x is measured from the center of the leading edge around the surface of the rectangular cylinder in the clockwise direction. The dashed curves represent the cases when the free surface effects play a dominant role as discussed above. Fig. 12(a) shows that the vorticity distributions on the leading edge ($0 \leq x \leq 0.5$, $3.5 \leq x \leq 4.0$) and lower surface ($2.5 \leq x \leq 3.5$) of the square have small differences as d/l decreases from 1.0 to 0.3. However, on the upper surface ($0.5 \leq x \leq 1.5$) and trailing edge ($1.5 \leq x \leq 2.5$), distributions of the vorticity vary significantly as d/l varies. As shown in Fig. 12(a), with the decrease of d/l , the vorticity on the upper surface vary from negative values to positive values and the vorticity on the trailing edge decrease in magnitude. It is seen that when d/l is 0.3 and 0.5, the vorticity distributions around the square are different from those at other d/l values. This indicates the change of the flow as shown in Fig. 10. Similar phenomenon can be observed when w/l is 3.0. As shown in Fig. 12(b), the vorticity distributions on the upper surface ($0.5 \leq x \leq 3.5$) and trailing edge ($3.5 \leq x \leq 4.5$) at $d/l = 0.3$, $d/l = 0.7$ and $d/l = 0.8$ are different from those at $d/l = 0.9$ and $d/l = 1.0$. The results are appropriate reflections of the flow variations with the depth as shown in Fig. 11.

Based on the above discussions, it is predicted that there exists a critical depth-to-length ratio, below which the flow around rectangular cylinders is dominated by the free surface effects. As demonstrated by the flow visualizations, when d/l is larger than the critical value, the flow past rectangular cylinders shares similar features to those in an infinite domain; however, when d/l is lower than that value, totally different features of the flow are displayed. Discussions on the vorticity distributions around the rectangular cylinder at various depths confirm the prediction. Moreover, the critical depth-to-length ratio is found to be related to the width-to-length ratio of the rectangular cylinder. As presented above, the critical depth-to-length ratios for the rectangular cylinder with width-to-length ratios of 1.0 and 3.0 are in the ranges from 0.5 to 0.6 and from 0.8 to 0.9, respectively. A deep investigation on the relationship between the critical depth-to-length ratio and the width-to-length ratio is not carried out in the present study and is left for future works.

4.3. Effect of the width-to-length ratio

The effect of the width-to-length ratio on the flow past rectangular cylinders near the free surface is discussed in this section. Two depths ($0.3l$ and $0.6l$) of rectangular cylinders are considered. As discussed in the previous section, 0.6 approximates the critical depth-to-length ratio for the rectangular cylinder with the width-to-length ratio of 1.0.

The force coefficients of the rectangular cylinder with different width-to-length ratios are shown in Fig. 13. The results for the cases with $d/l = 4.5$ are also presented. As shown in Fig. 13(a), when d/l is 0.3, the drag coefficient decreases linearly as w/l increases from 0.6 to 5.0. The variation trend is markedly different from that of the case with $d/l = 4.5$. It is anticipated that due to the strong free surface effects, the flow around rectangular cylinders at the depth of $0.3l$ is totally different from that in an infinite domain. When d/l is 0.6, the variations of the drag coefficient have different characteristics in different w/l ranges. As w/l increases from 0.6 to 1.5, the drag coefficient drops sharply and the curve approximates that of the cases with $d/l = 4.5$. The small differences between the results at $d/l = 0.6$ and $d/l = 4.5$ are most probably

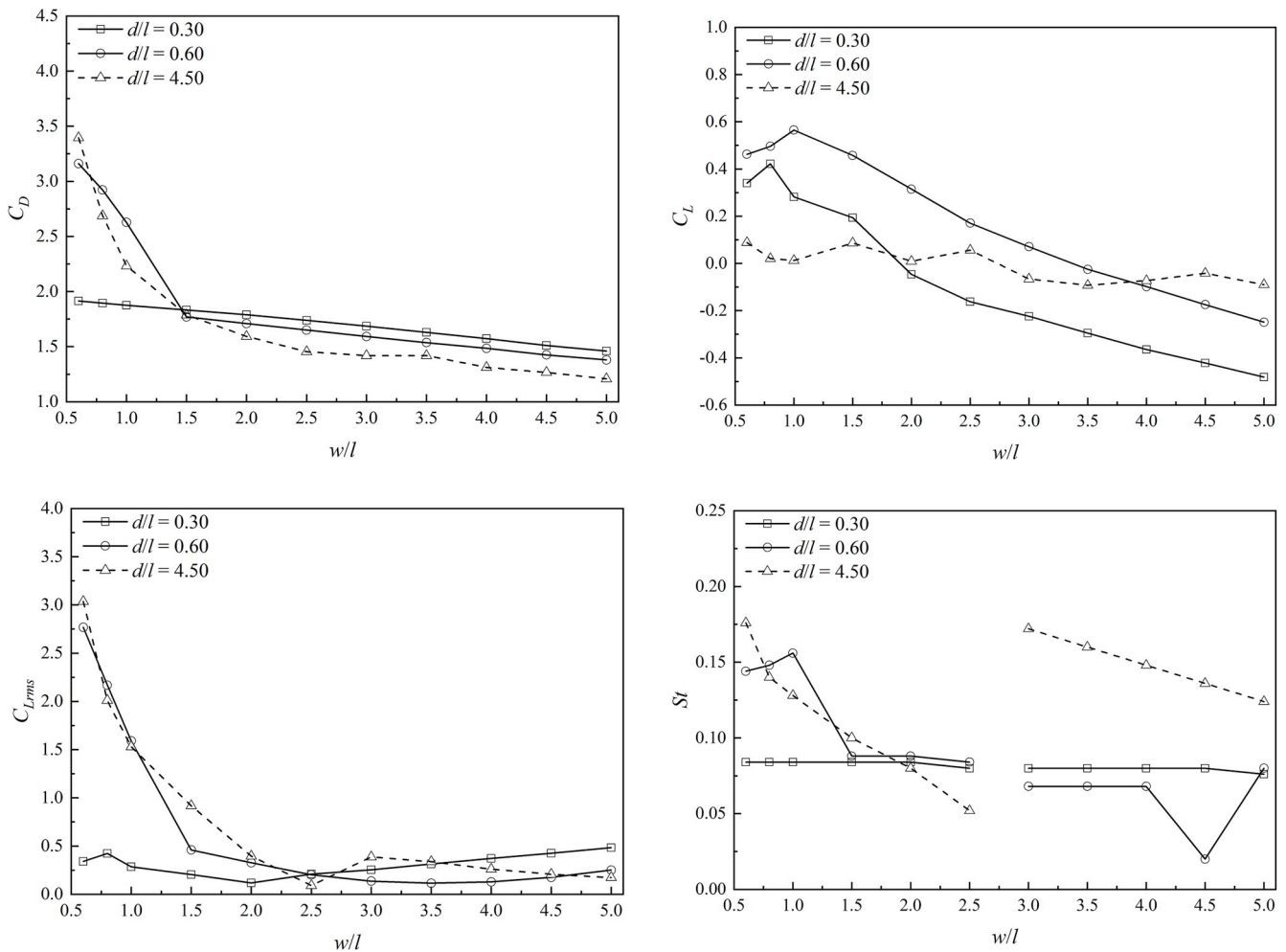


Fig. 13. Variations of the force coefficients of the rectangular cylinder with the width-to-length ratio: (a) Drag coefficient; (b) Lift coefficient; (c) Lift coefficient (r.m.s.); (d) Strouhal number.

due to the presence or absence of the free surface effects. As w/l increases from 1.5 to 5.0, the drag coefficient decreases slowly, with the declining curve paralleled to that of the cases with $d/l = 0.3$. It indicates that when the rectangular cylinder is located at the depth of 0.6 l , the interaction between the free surface and the vortex shedding is dramatically enhanced when w/l is larger than 1.5.

Fig. 13(b) shows that when d/l is 0.3, the lift coefficient decreases as w/l increases from 0.6 to 5.0. It is markedly different from that of the cases with $d/l = 4.5$, in which the lift coefficient varies slightly with w/l . When d/l is 0.6, the variations of the lift coefficient are different in different w/l ranges. As shown in Fig. 13(b), when w/l is lower than 1.5, the lift coefficient varies slightly as w/l increases, which is similar to that of the cases with $d/l = 4.5$. When w/l is larger than 1.5, the lift coefficient decreases with w/l , with the declining curve paralleled to that of the cases with $d/l = 0.3$. The distinct variation trends of the force coefficients in different w/l ranges at $d/l = 0.6$ can also be observed in the variations of the r.m.s. value of the lift coefficient as shown in Fig. 13(c). It is worth noting that the behaviors of the lift coefficient under varying w/l at the two depths ($d = 0.3l$ and $d = 0.6l$) are in accordance with those of the drag coefficient. Therefore, it is reasonable to predict that when d/l is 0.3, the interaction between the free surface and the rectangular cylinder is strong in the whole w/l range from 0.6 to 5.0, and the flow is dominated by the free surface effects. Due to this dominance, the variation trends of both the drag and lift coefficients with w/l are remarkably different from those when the rectangular cylinder is deeply submerged ($d/l = 4.5$). However, when d/l is 0.6, the flow past

rectangular cylinders is dominated by the free surface effects only at $w/l \geq 1.5$. when w/l is lower than 1.5, the interaction between the free surface and the rectangular cylinder is relatively less significant, and the features of the vortex shedding flow in an infinite domain are retained. This provides a good explanation for the different variation trends of the drag and lift coefficients in the two w/l ranges, i.e., from 0.6 to 1.5 and from 1.5 to 5.0.

Fig. 13(d) shows the variations of the Strouhal number with the width-to-length ratio. As shown in Fig. 13(d), when d/l is 0.3, the Strouhal number remains at a relatively low value ($St = 0.080$) when w/l increases from 0.6 to 5.0. This variation trend differs notably from that of the cases with $d/l = 4.5$. In particular, the discontinuity in the Strouhal number at around $w/l = 2.8$ is not present when the depth is 0.3 l . Observations on the flow structures reveal that throughout the whole w/l range from 0.6 to 5.0, the flow past rectangular cylinders located at the depth of 0.3 l displays totally different features from those in an infinite domain. Examples of this flow are shown in Figs. 10(a) and Fig. 11(a). It is important to note that $St = 0.080$ represents a typical characteristic of the vortex shedding suppressed by the free surface distortion, and can be used to identify the presence or absence of the dominance of the free surface effects. Fig. 13(d) also shows that when d/l is 0.6, the Strouhal number varies slightly as w/l increases from 0.6 to 1.0 and decreases sharply as w/l increases from 1.0 to 1.5. When w/l is larger than 1.5, the Strouhal number roughly remains at a value close to 0.080. It indicates that the free surface effects become dominant at $w/l \geq 1.5$. Observations on the flow structures confirm that when the depth

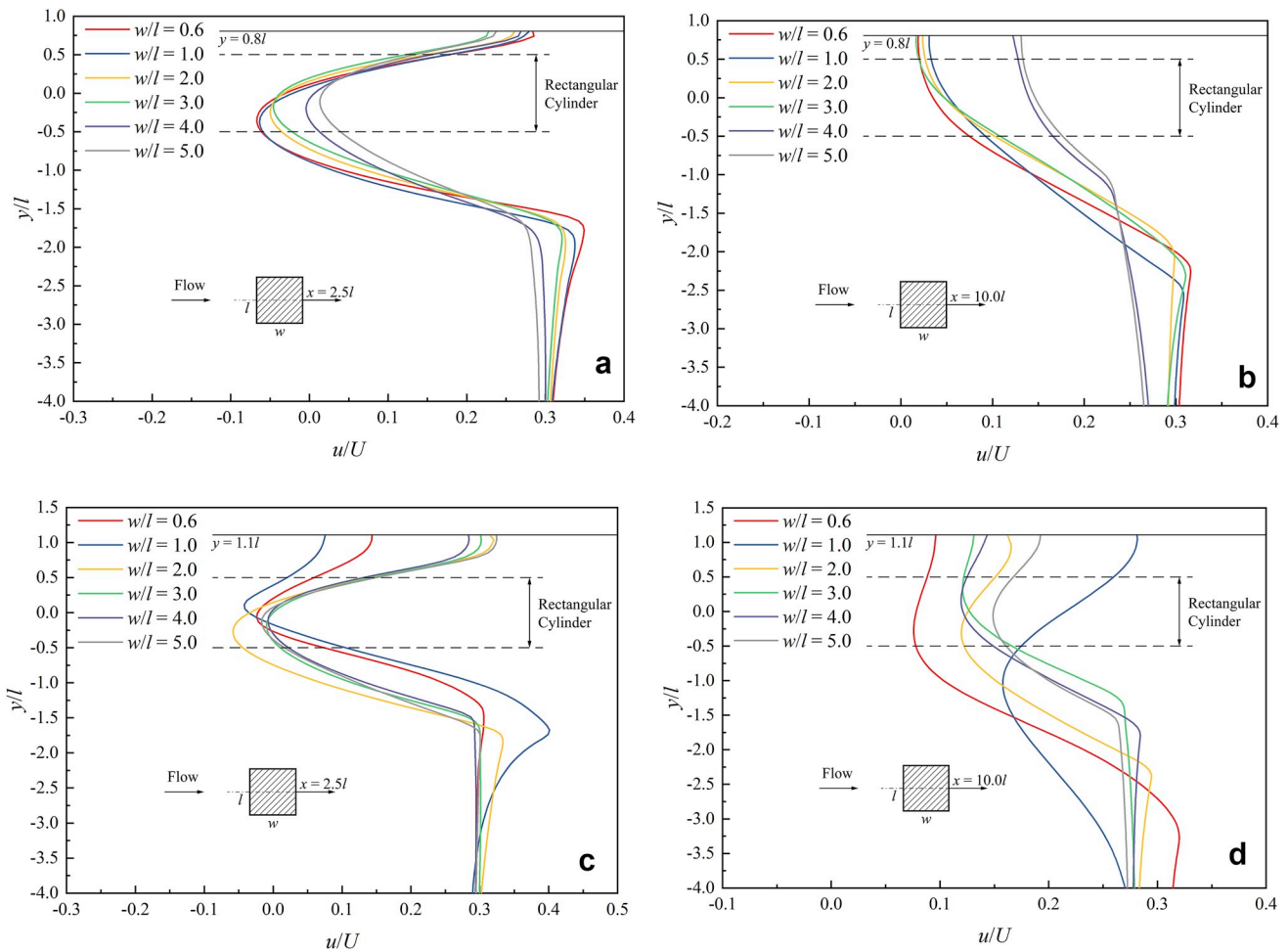


Fig. 14. Time-averaged streamwise velocity at two locations ($x = 2.5l$ and $x = 10.0l$) downstream the rectangular cylinder: (a) $x = 2.5l$ ($d/l = 0.3l$); (b) $x = 10.0l$ ($d/l = 0.3l$); (c) $x = 2.5l$ ($d/l = 0.6l$); (d) $x = 10.0l$ ($d/l = 0.6l$).

is $0.6l$, the flow past rectangular cylinders resembles that in an infinite domain at $w/l \leq 1.0$ and is dominated by the free surface effects at $w/l \geq 1.5$.

Fig. 14 shows the time-averaged streamwise component of the velocity at two locations ($x = 2.5l$ and $x = 10.0l$) downstream the rectangular cylinder. The distance x is measured from the center of the trailing edge. As shown in Fig. 14(a) and (b), the variations of the streamwise velocity with the depth at $x = 2.5l$ and $x = 10.0l$ are different. The sharp decrease of the streamwise velocity (at $x = 2.5l$) as y/l varies from 0.5 to -0.5 indicates that it is located in the recirculation region behind the rectangular cylinder. It is also seen from Fig. 14(a) and (b) that the streamwise velocity at different w/l values varies similarly with the depth. This demonstrates that the flow around the rectangular cylinder at the depth of $0.3l$ shares similar features as w/l increases from 0.6 to 5.0 . When d/l is 0.6 , the variations of the streamwise velocity with the depth change as w/l changes. As shown in Fig. 14(c) and (d), the streamwise velocity at $x = 2.5l$ and $x = 10.0l$ experiences a sudden change as w/l increases from 1.0 to 2.0 . It is in accordance with the change of the flow past the rectangular cylinder at around $w/l = 1.5$ as mentioned above.

Variations of the time-averaged vorticity with the depth at two locations ($x = 0.5l$ and $x = 1.5l$) downstream the rectangular cylinder are also studied. Fig. 15(a) and (b) show that when d/l is 0.3 , the vorticity decrease sharply from a relatively large positive value to about zero as y/l varies from 0.5 to -0.5 and decrease further as y/l varies from -0.5 to -1.0 . Similar variations of the vorticity with the depth can be seen in Fig. 15(c) and (d) at $w/l \geq 2.0$. This corresponds to the flow which is

strongly affected by the free surface. However, when w/l is 0.6 and 1.0 , the time-averaged vorticity shows positive and negative values behind the rectangular cylinder at $x = 0.5l$ and $x = 1.5l$, respectively. It is a demonstration of the periodic vortex shedding, which is typical for flow past rectangular cylinders in an infinite domain.

5. Conclusions

Flow past rectangular cylinders in the vicinity of the free surface was investigated in the present study. Two-dimensional RANS simulations using the Mentor SST $k - \omega$ model were conducted. The applicability of the Mentor SST $k - \omega$ model in modeling flow around rectangular cylinders near the free surface was first discussed. The effects of the depth-to-length ratio and the width-to-length ratio on the hydrodynamic properties of rectangular cylinders were then analyzed. The following conclusions were drawn:

1. Multiphase simulations based on the Mentor SST $k - \omega$ model can provide reasonable predictions of the force coefficients of rectangular cylinders close to the free surface when w/l is larger than 0.7 . The flow around rectangular cylinders at various width-to-length ratios from 1.0 to 5.0 can be reasonably reproduced via using the Mentor SST $k - \omega$ model.

2. The effect of the depth-to-length ratio on the hydrodynamic properties of rectangular cylinders is affected by the width-to-length ratio. Variations of the drag and lift coefficients and the Strouhal number with d/l are similar for rectangular cylinders with width-to-length ratios of 1.0 and 3.0 , but the amplitudes of variation and the

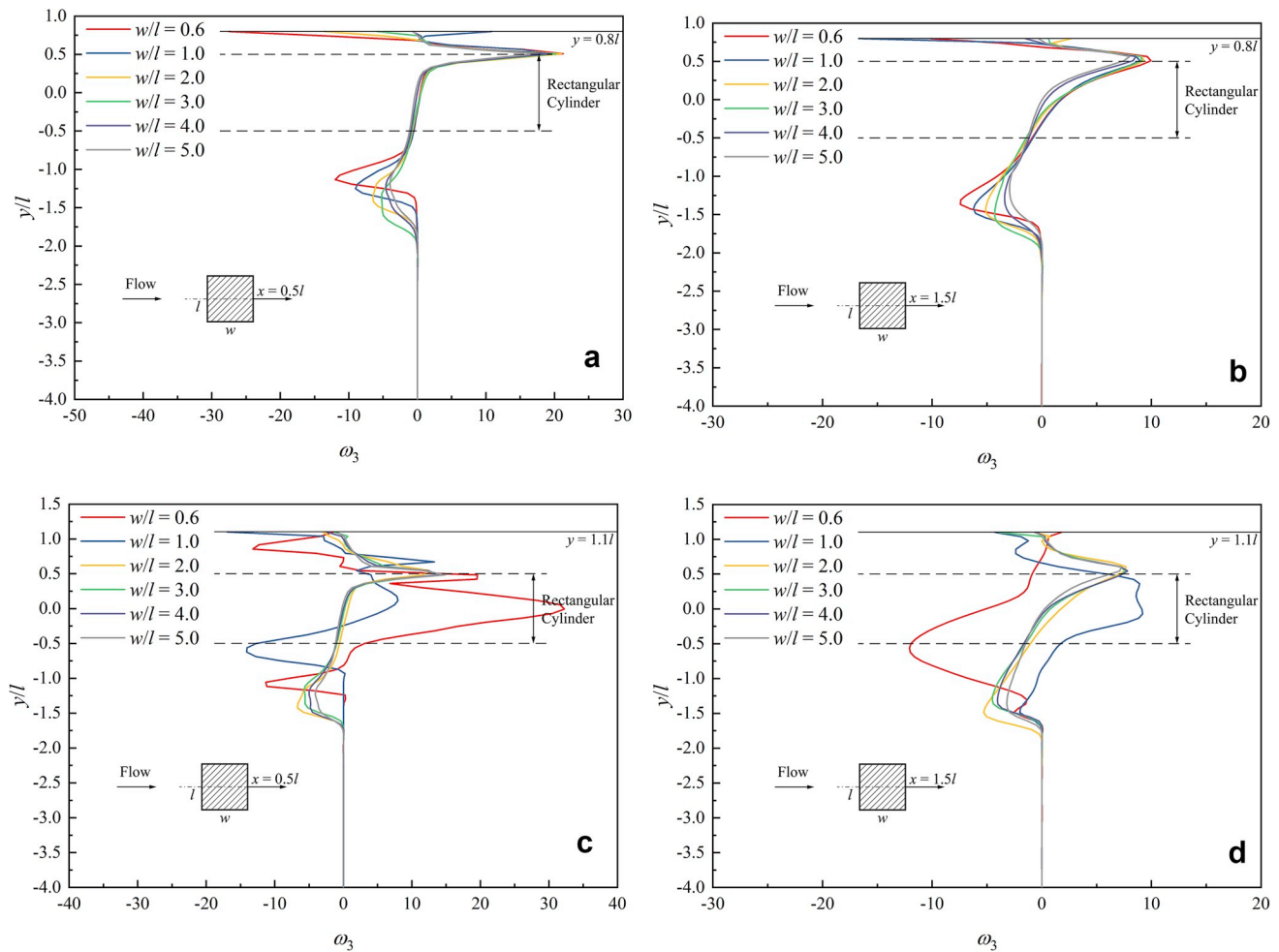


Fig. 15. Time-averaged vorticity at two locations ($x = 0.5l$ and $x = 1.5l$) downstream the rectangular cylinder: (a) $x = 0.5l$ ($d/l = 0.3l$); (b) $x = 1.5l$ ($d/l = 0.3l$); (c) $x = 0.5l$ ($d/l = 0.6l$); (d) $x = 1.5l$ ($d/l = 0.6l$).

corresponding ranges of d/l values are different. Specifically, the maximum drag coefficient ($C_d = 2.757$) of the rectangular cylinder ($w/l = 1.0$) appears at the depth of $0.8l$ while the maximum drag coefficient (at $w/l = 3.0$) is predicted to emerge in the extreme case of $d = 0$.

3. The free surface effects on the flow past rectangular cylinders become significant when the depth is lower than $1.0l$. This is reflected by the sharp rise of the lift coefficient in the d/l ranges from 1.0 to 0.6 and from 1.0 to 0.8 for rectangular cylinders with width-to-length ratios of 1.0 and 3.0, respectively. The substantial change of the flow occurs at around the depth of $0.6l$ and $0.9l$ for rectangular cylinders with width-to-length ratios of 1.0 and 3.0, respectively. The relatively low values of Strouhal number in the d/l ranges from 0.5 to 0.3 and from 0.8 to 0.3 for rectangular cylinders at $w/l = 1.0$ and $w/l = 3.0$ imply that at these d/l ranges, the free surface effects play a dominant role on the vortex shedding around rectangular cylinders.

4. There exists a critical depth-to-length ratio for rectangular cylinders located near the free surface. When d/l is larger than the critical value, the flow past rectangular cylinders shares similar features to those in an infinite domain; however, when d/l is lower than that value, the flow becomes dominated by the free surface effects. The critical depth-to-length ratios for the rectangular cylinder with width-to-length ratios of 1.0 and 3.0 locate in the ranges from 0.5 to 0.6 and from 0.8 to 0.9, respectively. The relationship between the critical depth-to-length ratio and the width-to-length ratio remains to be investigated.

5. The effect of the width-to-length ratio on the flow past rectangular cylinders close to the free surface is different from that in an infinite domain. When d/l is 0.3, the flow past rectangular cylinders is

dominated by the free surface effects throughout the whole w/l range from 0.6 to 5.0 and the variation trends of the force coefficients are remarkably different from those in an infinite domain. A typical characteristic of the vortex shedding suppressed by the free surface distortion is the low Strouhal number ($St = 0.080$) which can be used to identify the presence or absence of the dominance of the free surface effects. When d/l is 0.6, the variations of the force coefficients have different characteristics at $w/l \leq 1.0$ and $w/l \geq 1.5$, and the change of the variation trends at $w/l = 1.5$ corresponds to the substantial change of the flow.

Acknowledgement

This work is supported by National Natural Science Foundation of China (NSFC) and China Scholarship Council (CSC). These supports are gratefully acknowledged. The first author also acknowledges the support from the School of Civil and Construction Engineering at Oregon State University where the first author is a visiting doctorate student.

Appendix A. Supplementary data

Supplementary data to this article can be found online at <https://doi.org/10.1016/j.oceaneng.2019.106118>.

References

- Bosch, G., Rodi, W., 2015. Simulation of vortex shedding past a square cylinder with different turbulence models. *Int. J. Numer. Methods Fluids* 28 (4), 601–616.
- Farhadi, M., Rahnema, M., 2005. Three-dimensional study of separated flow over a square cylinder by large eddy simulation. *Proc. IME G J. Aero. Eng.* 219 (G3), 225–234.
- Hirt, C.W., Nichols, B.D., 1981. Volume of fluid (VOF) method for the dynamics of free boundaries ☆. *J. Comput. Phys.* 39 (1), 201–225.
- Holzmann, T., 2016. *Mathematics, numerics, derivations and OpenFOAM®*. Loeben, Germany: holzmann CFD. URL: https://holzmann-cfd.de/visited_on_Nov.29.2017 (visited on Nov. 29, 2017).
- Jones, W.P., Launder, B.E., 1972. The prediction of laminarization with a two-equation model of turbulence. *Int. J. Heat Mass Transf.* 15 (2), 301–314.
- Liu, I.H., Riglin, J., Schleicher, W.C., Oztekin, A., 2016. Flow past a plate in the vicinity of a free surface. *Ocean Eng.* 111, 323–334.
- Lyn, A., Einav, D.S., Rodi, W., Park, J.H., 2006. A laser-Doppler velocimetry study of ensemble-averaged characteristics of the turbulent near wake of a square cylinder. *J. Fluid Mech.* 304 (304), 285–319.
- Malavasi, S., Guadagnini, A., 2003. Hydrodynamic loading on river bridges. *Journal of Hydraulic Engineering-Asce* 129 (11), 854–861.
- Malavasi, S., Guadagnini, A., 2007. Interactions between a rectangular cylinder and a free-surface flow. *J. Fluids Struct.* 23 (8), 1137–1148.
- Mannini, C., Soda, A., Schewe, G., 2010. Unsteady RANS modelling of flow past a rectangular cylinder: investigation of Reynolds number effects. *Comput. Fluid* 39 (9), 1609–1624.
- Mannini, C., Soda, A., Schewe, G., 2011. Numerical investigation on the three-dimensional unsteady flow past a 5:1 rectangular cylinder. *J. Wind Eng. Ind. Aerodyn.* 99 (4), 469–482.
- Menter, F.R., 1994. Two-equation eddy-viscosity turbulence models for engineering applications. *AIAA J.* 32 (8), 1598–1605.
- Miranda, D., Plantamura, A.V., Malavasi, S., 2013. Boundaries influence on the flow field around an oscillating sphere. In: *ASME 2013 32nd International Conference on Ocean, Offshore and Arctic Engineering*. American Society of Mechanical Engineers. V007T08A074–V007T08A074.
- Miyata, H., Shikazono, N., Kanai, M., 1990. Forces on a circular cylinder advancing steadily beneath the free-surface. *Ocean Eng.* 17 (1), 81–104.
- Mizota, T., Yamada, H., Kubo, Y., Okajima, A., Knisely, C.W., Shirato, H., 1988. Aerodynamic characteristics of fundamental structures (Part 1). *Wind Engineers, JAWE* 1988 (36), 50–79.
- Moukalled, F., Mangani, L., Darwish, M., 2015. *The Finite Volume Method in Computational Fluid Dynamics: an Advanced Introduction with OpenFOAM and Matlab*. Springer Publishing Company, Incorporated.
- Murakami, S., Mochida, A., 1995. On turbulent vortex shedding flow past 2D square cylinder predicted by CFD. *Journal of Wind Engineering & Industrial Aerodynamics* s 54–55 (94), 191–211.
- Nakaguchi, H., Hashimoto, K., Muto, S., 1968. An experimental study on aerodynamic drag of rectangular cylinders. *J. Jpn. Soc. Aeronaut. Space Sci.* 16 (168), 1–5.
- Norberg, C., 1993. Flow around rectangular cylinders: pressure forces and wake frequencies. *J. Wind Eng. Ind. Aerodyn.* 49 (1–3), 187–196.
- Ohtsuki, Y., 1978. Wind tunnel experiments on aerodynamic forces and pressure distributions of rectangular cylinders in a uniform flow. In: *Proc. 5th Symp. On Wind Effects on Structures*, pp. 169–175.
- Ong, M.C., Utnes, T., Holmedal, L.E., Myrhaug, D., Pettersen, B., 2009. Numerical simulation of flow around a smooth circular cylinder at very high Reynolds numbers. *Mar. Struct.* 22 (2), 142–153.
- Reichl, P., Hourigan, K., Thompson, M.C., 2005. Flow past a cylinder close to a free surface. *J. Fluid Mech.* 533, 269–296.
- Sakamoto, H., Haniu, H., Kobayashi, Y., 1989. Fluctuating forces acting on rectangular cylinders in uniform flow : on rectangular cylinders with fully separated flow. *Nihon Kikai Gakkai Ronbunshu B Hen/transactions of the Japan Society of Mechanical Engineers Part B* 55 (516), 2310–2317.
- Schewe, G., 2013. Reynolds-number-effects in flow around a rectangular cylinder with aspect ratio 1:5. *J. Fluids Struct.* 39 (5), 15–26.
- Shimada, K., Ishihara, T., 2002. Application of a modified $k - \epsilon$ model to the prediction of aerodynamic characteristics of rectangular cross-section cylinders. *J. Fluids Struct.* 16 (4), 465–485.
- Shur, M., Spalart, P.R., Squires, K.D., Strelets, M., Travin, A., 2005. Three dimensionality in Reynolds-averaged Navier-Stokes solutions around two-dimensional geometries. *AIAA J.* 43 (6), 1230–1242.
- Sohankar, A., 2008. Large eddy simulation of flow past rectangular-section cylinders: side ratio effects. *J. Wind Eng. Ind. Aerodyn.* 96 (5), 640–655.
- Stringer, R.M., Zang, J., Hillis, A.J., 2014. Unsteady RANS computations of flow around a circular cylinder for a wide range of Reynolds numbers. *Ocean Eng.* 87 (5), 1–9.
- Tamura, T., Itoh, Y., 1996. Aerodynamic characteristics and flow structures around a rectangular cylinder with a section of various depth/breadth ratios. *Journal of Structural & Construction Engineering* 61 (486), 153–162.
- Tian, X.L., Ong, M.C., Yang, J.M., Myrhaug, D., 2013. Unsteady RANS simulations of flow around rectangular cylinders with different aspect ratios. *Ocean Eng.* 58 (58), 208–216.
- Wilcox, D.C., 2006. *Turbulence modeling for CFD*. DCW industries.